STRATEGIES FOR ENHANCING THE MECHANICAL DURABILITY OF TRANSPARENT SUPERHYDROPHOBIC COATING AND DEVELOPMENT OF COLOR AND DURABLE SUPERHYDROPHOBIC PAINT

By

YUNG CHIEH HUNG

A DISSERTATION PRESENTED TO THE GRADUATE SCHOOL OF THE UNIVERSITY OF FLORIDA IN PARTIAL FULFILLMENT OF THE REQUIREMENTS FOR THE DEGREE OF DOCTOR OF PHILOSOPHY

UNIVERSITY OF FLORIDA

2016

To the family and friends that helped me make it through

ACKNOWLEDGMENTS

I would like to thank my advisor Dr. Sigmund and the members of Sigmund group. We learned new things by brainstorming every day that I have spent here on University of Florida. I also would like to thank my parents and my wife because they always encouraged me when I was down. Without their assistance, I may not have been able to make it through.

TABLE OF CONTENTS

LIST OF TABLES

LIST OF FIGURES

LIST OF ABBREVIATIONS

CB state	Cassie-Baxter state
CDR	Coating depletion rate
DMF	Dimethylformamide
EtAc	Ethyl acetate
MPTMS	(3-Mercaptopropyl) trimethoxysilane
PMMA	Polymethyl methacrylate
PVDF	Polyvinylidene difluoride
SH	Superhydrophobic
SBS	Standard binder solution
UV	Ultraviolet
WCA	Water contact angle

Abstract of Dissertation Presented to the Graduate School of the University of Florida in Partial Fulfillment of the Requirements for the Degree of Doctor of Philosophy

STRATEGIES FOR ENHANCING THE MECHANICAL DURABILITY OF TRANSPARENT SUPERHYDROPHOBIC COATING AND DEVELOPMENT OF COLOR AND DURABLE SUPERHYDROPHOBIC PAINT

By

Yung-Chieh Hung

August 2016

Chair: Wolfgang Sigmund
Major: Materials Science and Engineering

Superhydrophobic surfaces feature repellency of liquids and enhance existing or enable novel technologies such as self-cleaning, have anti-fouling behavior, and icephobicity. Superhydrophobicity is quantitatively described by surface science theories such as the Cassie Baxter model. From this model it is obvious that changes in the surface chemistry due to oxidation or surface topography due to abrasion or aging causes the coating to lose its superhydrophobic property. This lack of durability in products currently limits the commercial breakthrough of this technology. This dissertation addresses four major objectives. 1) Development of a quantitative durability test that could be standardized. 2) Develop a composite paint for durability. 3) Understand the structure of durable superhydrophobic coatings. 4) Apply this knowledge to build the ultimate coating which is superhydrophobic, durable and transparent. Such a coating could be applied to any material or device without changing its looks and is most desired by a large number of companies throughout the world.

This dissertation addresses the above mentioned challenges first by developing and then testing and applying a new wear resistance measurement approach for superhydrophobic

coatings, which could be used for standardization in this field. It is built on existing ASTM standards (ASTM D4060 – 14) with modifications for superhydrophobic surfaces. Moreover, the advances achieved by using this standard for characterizing samples allowed the development of novel superhydrophobic coatings that are durable. The concept that was applied is based on capillary and funicular structures in mostly dense composite materials consisting of hydrophobic polymers with hydrophobic ceramic particles. The volumetric thick thermoplastic component of the paint layer gives it the mechanical strength to achieve superhydrophobicity through 1000 abrasion cycles by metallurgical sand paper. The scalability was addressed by formulating this coating as a paint. This allows for application in large areas, and the possibility to add colors beyond white, which in this work are black, blue, green and red. The concept allows to fabricate any other type of colored paint as long as the pigments can be hydrophobized or are themselves already hydrophobic. By varying the particle volume percent, threshold to achieve superhydrophobicity could be demonstrated in this way. This research states the threshold to attain superhydrophobicity is around 60V%-70V% of particle no matter what pigments were selected. This value is also the transition point from capillary structure to funicular structure.

The application of this breakthrough to transparent SH coatings is of course more challenging. In order to achieve durable and transparent SH coating, novel approaches are reported in this dissertation. Moving from an organic-inorganic paint system to a ceramic-ceramic system allows to reduce scattering induced by the variation in refractive indices of the components. A silica sol-gel is used to enhance mechanical and chemical bonding of nanoparticles. Threshold to achieve superhydrophobicity is also located in 60V% to 70V% and fulfill our expectation. Moreover, a second novel concept using particle agglomeration and bonding to enhance transparent superhydrophobic material is introduced. Monodisperse silica

nanoparticles were treated with a variety of silane coupling agents. By doing so, the silica nanoparticles became functionalized with reactive groups that allowed bonding under specific conditions. The introduction of directly chemically bonding particles further enhanced the durability. However, a lot more needs to be done since the scattering limits of the materials in composites or just the surface features alone make it challenging to provide the proper surface architecture and chemistry while being mechanically robust to withstand abuse.

In summary this work advances the field of superhydrophobic coatings, applies the theories and standards for characterization, and demonstrates them in examples of novel durable ceramic-polymer and transparent ceramic-ceramic composite coatings.

CHAPTER 1
SUPERHYDROPHOBIC AND HYDROPHOBIC MATERIALS

Introduction

Superhydrophobicity was discovered from natural phenomenon, the most famous of these being the lotus effect[1]–[6]. Superhydrophobic (SH) materials are versatile and possess fascinating properties such as:

- **1. Self-cleaning property** [7]–[13] This is one of the most important phenomena of superhydrophobic surfaces. When a water droplet rolls off the surface, it picks up dirt and keeps the surface clean. Superhydrophobic coatings could keep surfaces clean via flushing by natural raining, reducing consumption of water. Namely, SH material can be considered a green material.
- **2. Anti-biofouling surfaces**: With lower surface energy, SH material can reduce the displeasing adherence of bacterial and bio-films. SH materials have the potential to replace toxic coatings used in marine applications, such as tributyltin (TBT) and triphenyltin (TPT)[14].
- **3. Drag force reduction**: In the cassie-baxter state, a thin layer of air is trapped between the SH surface and water. So partial interaction between solid and liquid vanishes, and this reduction can be as high as 50%[15]. With water repellent coatings on the surface, watercraft could be more energy efficient.

Given these advantages, SH materials have attracted researchers' attention in the last decade. Theoretically, a super-hydrophobic surface is defined as a surface where the water contact angle (WCA) is greater than 150° and the roll–off, or sliding angle is less than 10° tilt from horizontal. Literature has demonstrated that the basic theory of superhydrophobicity can be divided into two main sections[3], [5], [6], [16], [17].Surface roughness, or morphology, and the lotus effect are mainly built on this concept. Tiny protrusions on the lotus or taro leaves provide a high roughness factor and result in contact angles being >150° and self –cleaning properties.

Secondly, not only does roughness play an essential role, so does surface chemistry. Without proper chemistry, a surface loses self-cleaning or other SH properties, even though it has high contact and sliding angles. In this situation, also called the Wenzel state, the surface loses its superhydrophobic characteristics. Therefore, surface chemistry determines whether the

surface can reduce the attraction between water and surface, and low surface energy chemicals or materials must be selected to achieve superhydrophobicity.

Wetting Theory

Surface Tension

Surface tension is caused by an imbalance of attractive forces at the surface, where atoms, molecules or ions are surrounded by a reduced number of similar materials or have larger distances to their nearest neighbors. For liquids, this results in the molecules on the surface being energetically unstable. Therefore, the surface creates a force to try to minimize the number of dangling bonds and its free surface area. This force is known as the surface tension (γ) in fluid systems or free surface energy in solid materials. These units can be interpreted either as tension force per unit length of a line (e.g. N/m) or as energy per unit surface area (J/m^2) at the surface.

Wetting Equilibria

In terms of contact between two substances, there are multiple types of wetting, no matter those substances are liquid or solid. Three types of wetting are reported by Osterhuf, 1930, which are: (1) spreading wetting, (2) adhesion wetting, and (3) immersional wetting.

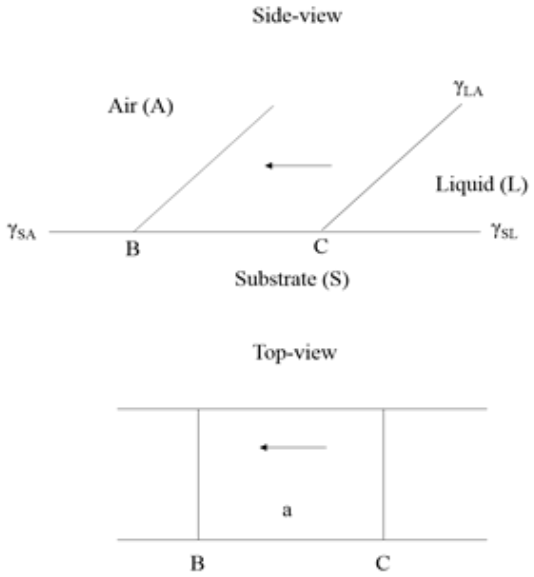

Figure 1-1. Spreading wetting

In Figure 1-1, the liquid-air interface moving from point C to point B causes a change in the surface energy of the whole system. For spreading to occur spontaneously, the energy change should be negative. The energy change is $\Delta G_w = -a \times \gamma_{SA} + a \times (\gamma_{SL} + \gamma_{LA})$ because the system loses solid – air interface and gains solid-liquid, liquid –air interface by area a. Because area term "a'' is always positive, the spreading coefficient is defined:

$$-\Delta G_w / a = S_{L/S} = \gamma_{SA} - (\gamma_{SL} + \gamma_{LA}) \quad (1\text{-}1)$$

The term $\gamma_{SA} - (\gamma_{SL} + \gamma_{LA})$,the spreading coefficient, is the driving force and determines whether the spreading process occurs spontaneously or not. If $S_{L/S} > 0$, liquid will spread over the whole substrate. If $S_{L/S} < 0$, liquid will stop spreading at a certain point, which is where contact angle comes in.

Contact Angle

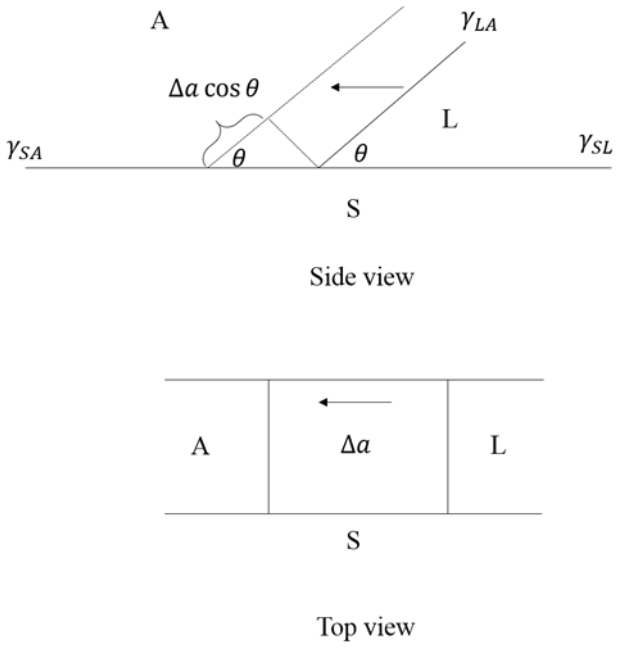

Figure 1-2. Contact angle

While substrate is solid, liquid wets the surface and forms a spherical cap with static contact angle θ; this value is determined by the equilibrium of surface energy from three phases

(Figure 1-2). For a trivial move in the position on the surface, there is an area increase Δa in the L/S interface, an area increase $\Delta a \cos\theta$ in the L/A interface, but an area decrease Δa in the S/A interface. Hence, the energy change could be calculated as

$$\Delta G_w = -\gamma_{SA}\Delta a + \gamma_{SL}\Delta a + \gamma_{LA}\cos\theta\Delta a \quad (1\text{-}2)$$

if $\Delta a \to 0, \Delta G_w = 0$ this equation can be rewritten as

$$\gamma_{LA}\cos\theta = \gamma_{SA} - \gamma_{SL} \quad (1\text{-}3)$$

$$\cos\theta_c = \frac{\gamma_{SA}-\gamma_{SL}}{\gamma_{LA}} \quad (1\text{-}4)$$

This equation is called Young's equation. If the value of the static CA is $0^\circ \leq \theta_c \leq 90°$, the liquid tends to spread on the surface. It is usually referred to as hydrophilic or oleophilic surface in terms of aqueous or oily liquid, respectively. If the value of the contact angle is $90°^\circ \leq \theta_c \leq 180°$, the wetting area tends to shrink and forms a spherical droplet. If the CA is over 150°, the surface is referred to as superhydrophobic.

Classical Models for Contact Angles on Rough Surfaces- Wenzel State

The Wenzel model considers a homogeneous solid-liquid interface where the solid surface is rough. However, Young's equation is an oversimplified expression and only considers ideally flat surfaces that are atomically smooth and chemically homogeneous. In reality, very few solids are atomically smooth. Therefore, the roughness should be taken into consideration. In the Wenzel state, where the roughness is completely filled with liquid, the water contact angle in Wenzel state (θ_w) can be described by:

$$\cos\theta_w = R_f \times \cos\theta_c \quad (1\text{-}5)$$

Where R_f is called the roughness factor which is defined as:

$$R_f = \frac{Actual\ area}{Projected\ area} \tag{1-6}$$

Since R_f is always positive when the CA is less than 90^0, the roughness factors cause smaller contact angles; however, if the CA is larger than 90^0, the R_f causes a larger contact angle. In other words, the roughness factor makes hydrophilic surfaces more hydrophilic and hydrophobic surfaces more hydrophobic.

Heterogeneous Solid- Liquid Interface: Cassie-Baxter Model

Furthermore, the Wenzel regime is usually recognized as homogeneous wetting, since the liquid completely penetrates the grooves. Yet, under superhydrophic circumstances, vapor pockets may become trapped underneath the liquid yielding a composite surface (Figure 1-3c). This heterogeneous wetting is illustrated by Cassie-Baxter theory, where the contact angle can be predicted by equation:

$$\cos(\theta_{CB}) = f_s \cdot \cos(\theta_c) + f_v \cdot \cos(\theta_v) \tag{1-7}$$

Where θ_c is the theoretical contact on the smooth surface which is defined by the Young's equation, and f_s and f_v are the contact area fraction of the solid and vapor. Because $f_s + f_v = 1$ and $\theta_v = 180°$ (because liquid droplet in the air is a perfect sphere), this equation could be modified to:

$$\cos(\theta_{CB}) = f_s \cdot (\cos(\theta_c) + 1) - 1 \tag{1-8}$$

From Eq.1-7 and Eq.1-8, the lesser contact area of liquid to solid substrate leads to a higher contact angle in the Cassie-Baxter state (usually suitable when water contact angle is higher than 150°). With this equation, f_s could be calculated once $\cos(\theta_{CB})$ is measured. The calculation value listed in this dissertation was based on this equation.

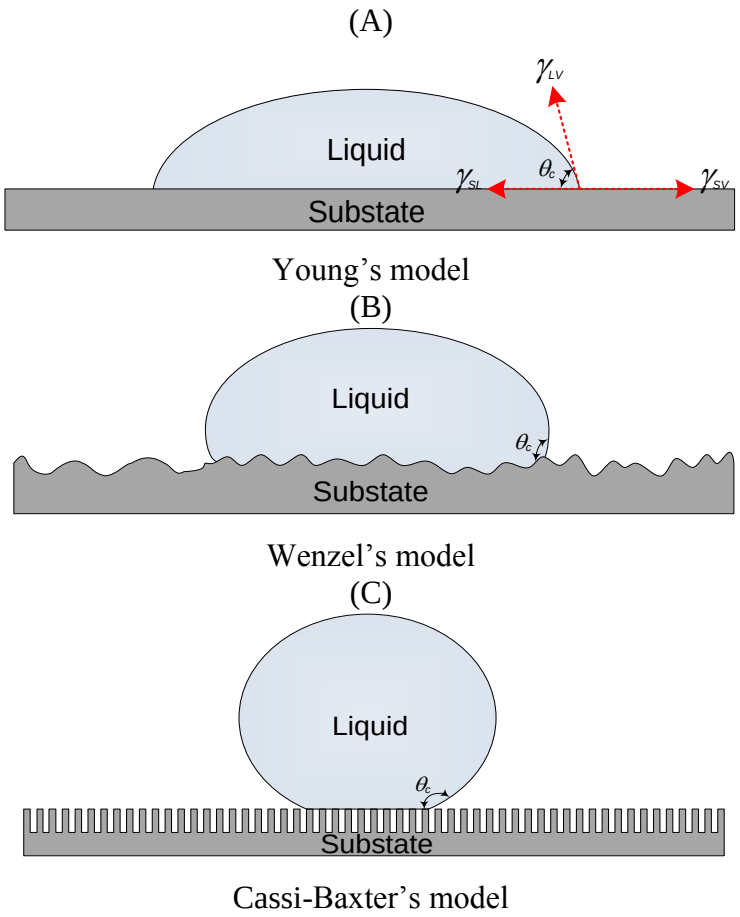

Figure 1-3. Wetting behavior of a liquid droplet on solid surface and their mathematical models. A) A liquid droplet on an ideally flat surface, Young's equation, B) Liquid droplet on a rough surface, Wenzel model, C) Vapor pockets are trapped between the grooves and the liquid droplet, Cassie-Baxter model.

Contact Angle Hysteresis

While the preceding section is for the static contact angle model, there is another method to evaluate the superhydrophobicity. The contact angle hysteresis is also an essential characteristic of a solid-liquid interface that is affected by the roughness and chemical inhomogeneity of a surface. Superhydrophobic coatings should not only have high contact angle but also low contact angle hysteresis and sliding angle.

Contact angle hysteresis, θ_{hys}, is defined by Eq.

$$\theta_{hys} = \Delta\theta = \theta_{adv} - \theta_{rec} \quad (1\text{-}9)$$

θ_{adv} and $\theta_{rec}$are the advancing angle and the receding angle, respectively. The advancing angle is the maximum value of contact angle before the liquid-solid contact line begins to advance; contrarily, the receding angle is the minimum value of contact angle before retreat. Hence, the static contact angle is always in this range which is $\theta_{adv} > \theta_c > \theta_{rec}$. Advancing and receding angle are usually measured by sessile drop measurements, where water is pumped into or withdrawn from a static droplet (Figure 1-4).

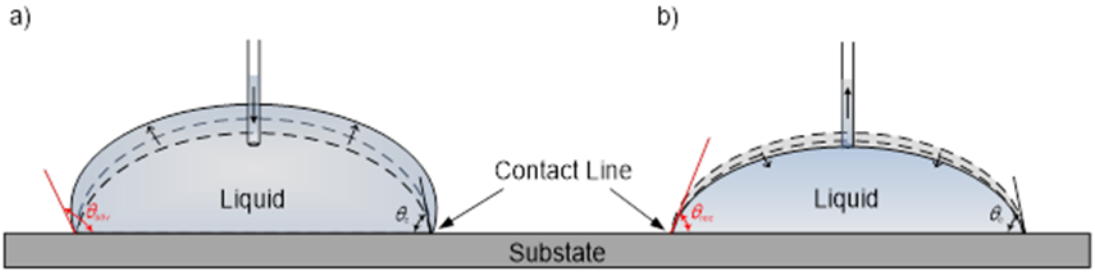

Figure 1-4. Contact angle hysteresis. A) Advancing angle (θ_{adv}) is the maximum contact angle of a droplet before its contact line (liquid-solid interface) starts advancing. B) Receding angle(θ_{rec}) is the minimum contact angle of a droplet before its contact line starts to receding.

Transition between Cassie-Baxter and Wenzel State

According to Equations 1-5 and 1-7, two contact angles are defined differently for a surface with one roughness condition. These two theories don't compete as the Cassie-Baxter state is a metastable state that only occurs in superhydrophobic regime. Several reports have mentioned solid/liquid contact mode shifted from Cassie-Baxter state to Wenzel state by external physical pressing[18], [19]. Jose et al [20]demonstrated the threshold value of Cassie-Baxter state to Wenzel state could be written as

$$\cos\theta_{trans} < \frac{f_s - 1}{r - f_s} \quad (1\text{-}10)$$

Where fs is the contact area fraction of solid and r is the roughness factor. Interestingly, fs is smaller than 1 and r is bigger than 1. These turn the right side of equation 1-8 to negative and means cosθ must be negative to make trapped air pockets stable. If Young's contact angle of solid is lower than the value given by eq. (1-8), trapped air pockets are not stable, and the Wenzel mode will dominate. To meet the criteria for the Cassie-Baxter state to exist, a solid substrate should either be hydrophobic enough or the roughness factor must be high.

Contact Angle Measurement

Contact angle measurement is carried out by acquiring images of resting drops on the surface through a specific apparatus, the goniometer. A goniometer could help us to measure the static water contact angle and contact angle hysteresis, as shown in Figure 1-5 below.

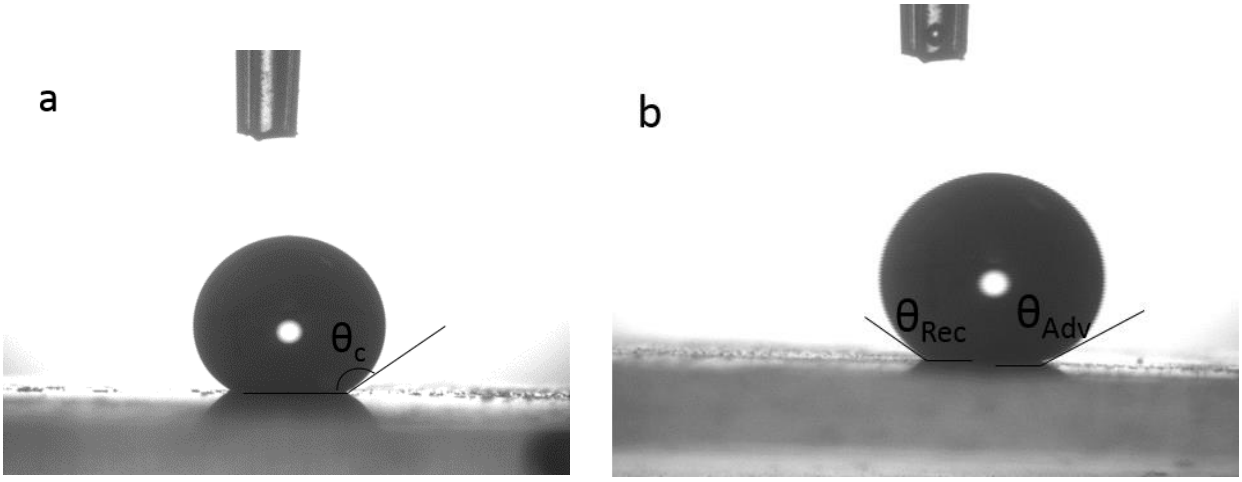

Figure 1-5. Image of contact angle measurement. A) Static water contact angle measurement. B) contact angle hysteresis measurement

$$\Delta\theta = \theta_{adv} - \theta_{rec} \quad (1\text{-}11)$$

However, a recognized protocol of measuring has not been established. Although using the same system and equipment, the results may change if the measurements are performed with slight variations. Hence, some factors should be taken into consideration:

1. **Drop size**: The drop size should be large enough compared to the surface features[21]. If the drop size is too large, the drop shape may be distorted by the gravity. Drops that are too small are difficult to be placed on the test surface, especially on a superhydrophobic sample. Generally, the standard is 10µl, and using the same size of drops throughout the whole measurement is essential.
2. **Drop placement**: Most of the tests for superhydrophobicity are located in the meta-stable, Cassie-Baxter state, regime where the drops are triggered to change to a more stable state, the Wenzel state, by external forces. The solution minimizes the kinetic energy of drops before taking images.
3. **Image quality**: Acquiring a clear image is probably the most crucial part of conducting the measurement. The background should be as clear as possible, especially on the bottom portion. This is challenging when dealing with superhydrophobic surfaces since the contact angle is high, and the drops have limited contact area on the surface. Sometimes, an extra light source is necessary to optimize the image quality.

All these factors are essential and should be taken into account during contact angle measurements. The key is to perform a measurement in the same conditions, and report the conditions and parameters clearly.

Traditional Superhydrophobic Surface Fabrication

Like previously mentioned, surface chemistry and surface roughness are two key factors needed for achieving superhydrophobicity. Briefly speaking, moulding and photolithography are typical approaches to build surface features.

Making Hairy Surface via Moulding Techniques:

Hsu et al [22] casted hairy structures made of micro-size polypropylene using track-etched polycarbonate membranes. Figure 1-6 shows the pore size of a commercial poly-carbonated membrane and the diameter was around 3 µm. They attached a polycarbonate membrane to a polypropylene substrate, and applied heat and pressure. Once the temperature surpassed the Tg of polypropylene, the PP substrate turned to plastic, which filled in the pores. Afterwards, the membrane was peeled off and the hairy polypropylene structure was obtained; the process flow is shown in Figure 1-7

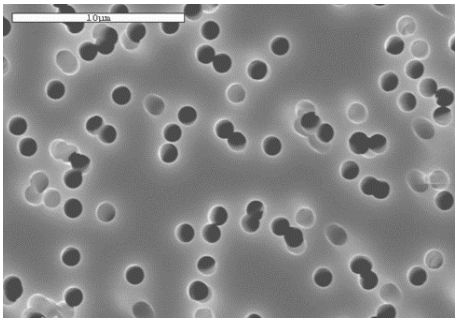

Figure 1-6.Commercial polycarbonate membrane with pore size 3µm.(Photo courtesy of Shu hau and Dr. Wolfgang Sigmund)

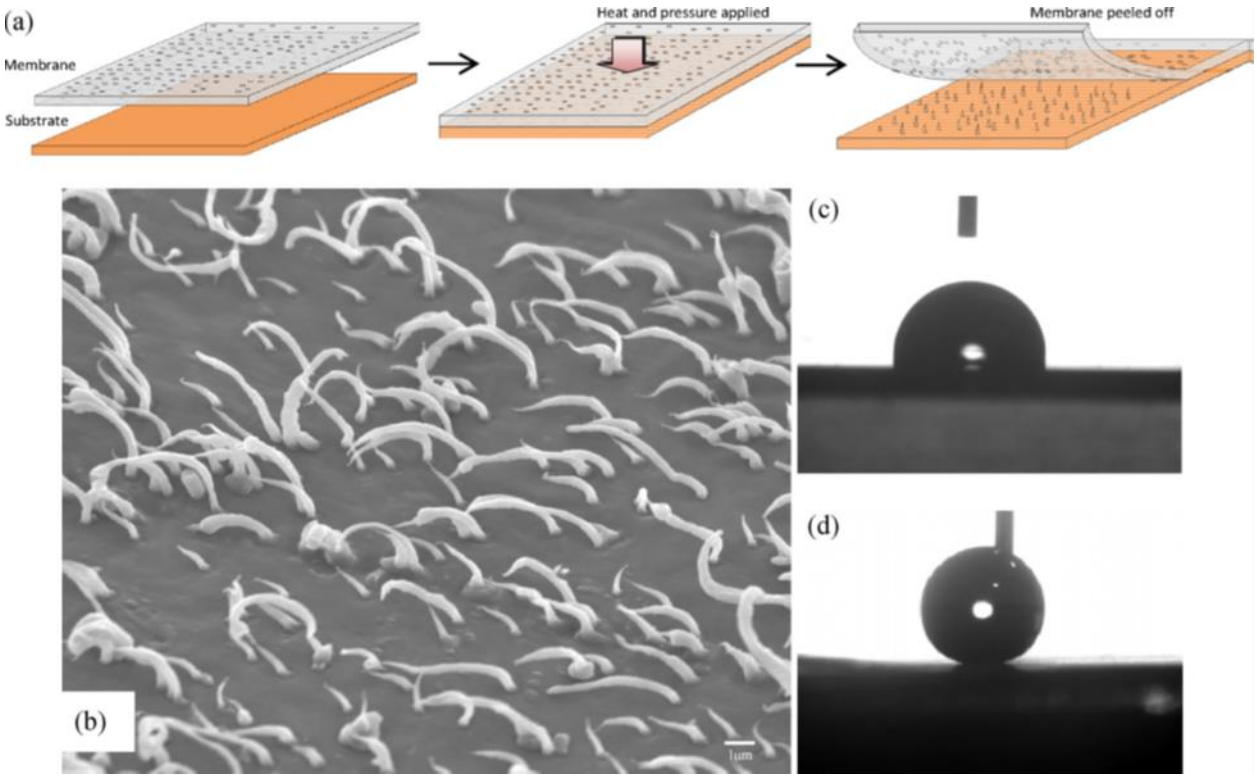

Figure 1-7. Fabrication of superhydrophobic from polypropylene. a) Process flow of PP hairy structure superhydrophobic surface) SEM image of hairy structure. c) Contact angle of PP flat surface.d) Contact angle of PP hairy structure surface (Photo courtesy of Shu hau and Dr. Wolfgang Sigmund)

Casting Fine Surface Structure via Photolithography

In the review paper written by P. Roach et al [23], they organized 9 reports which fabricated fine structures via photolithography. Fine structure is applicable to demonstrate the

superhydrophobic theory and discuss how roughness affects contact angle. With fine and shape-unitary structure, roughness could be calculated to prove Cassie-Baxter state to Wenzel state transition. However, photolithography is a costly approach and not scalable.

Current Limitations of Superhydrophobic Materials

Mechanical Durability

To conclude, plenty of papers have been posted which contain novel, creative approaches to fabricate superhydrophobic coatings and materials. Nevertheless, until recently, none of these were turned into a commercial product Simpson et al [24] reported possible reasons which are:

1. Cost issues: Because micro or even nano features are necessary for a superhydrophobic coating, most of the early research used photolithographic processes to fabricate the fine surface structure, which is costly and has limited applicability to greater area.

2. Nano structure stability and coating durability: Surface features are essential for superhydrophobic coatings.

However, these structures are vulnerable against shear force, and once the surface features are removed or destroyed, the surface turns hydrophobic only. Figure 1-8 shows a hairy structure of a polypropylene surface that was destroyed by a finger touch and lost superhydrophobicity. Micro structures on a silicon wafer were damaged by sand particles as shown in the SEM image in Figure 1-9. [19]

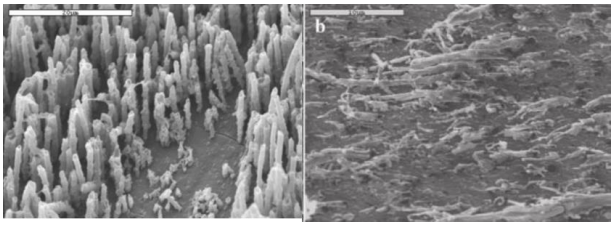

Figure 1-8.Superhydrophobic hairy polypropylene surface. a) Before finger touching. b) Surface was destroyed by the touch of a finger. Reprinted with permission from Hsu, S.-H.; Sigmund, W. M. Artificial Hairy Surfaces with a Nearly Perfect Hydrophobic Response. Langmuir 2010, 26, 1504–1506.23

Optical Property

Apart from mechanical wear resistance, superhydrophobic coating is usually blurry because of light scattering caused by surface roughness.Transparent superhydrophobic coatings could for example be applied on solar cell panels to keep them clean and at their highest efficiency[25]–[30]. Cars would not need washing as long as it rains sometimes and amount of bacteria, viruses and dust could be lowered overall in operating rooms and hospitals by such coatings. Several reports exist that demonstrated transparent superhydrophobic coatings using nanoparticles that are below the Fraunhofer and Mie scattering for light. However, all these coatings suffer from lack of durability. This is due to the oxidation of the materials and the low thickness of the coating. For the transmittance part, although some previous work has fabricated transparent and superhydrophobic coatings via lithographic procedures to create the nano-scale features on the substrate, this approach expresses distinct limitations for large-scale application. More recently, plentiful reports claim that superhydrophobic and transparent coating has been achieved and developed. Nevertheless, after scrutiny, the transmittance is not high enough (with most <90%) to be considered transparent.

Current Measurements for Mechanical Durability of Superhydrophobic Surface

Although some reports announced the development of durable superhydrophobic materials, techniques used to evaluate properties are inconsistent, and the standards regulating the conditions and information needed to be reported are absent. A brief summary of the techniques are shown in Table 1-1. Although researchers provided many ways to test the durability of superhydrophobic material. None of them is a quantitative way to depict the resistance of superhydrophobic material. Therefore, a new stand to describe the wear resistance of SH material is necessary.

Table 1-1. Current methods to measure wear resistance of SH material

Methods of Mechanical Wear
1. Sample rubbed against clothes [31]–[33]
2. Sample rubbed against sand paper [32], [34], [35]
3. Sample rubbed against synthetic leather under a certain load [36]
4. Sample Abraded by cotton swab[37]
5. Sample Abraded by steel wool
6. Ball on disk test[38]
7. Sand abrasion test [39]
8. Adhesive tape [40]
9. High speed current scouring or water jet test[41]

Table 1-2. Current methods to characterize wear resistance of SH material

Characterization of mechanical wear
1. Change in contact angle hysteresis [32]
2. Water shedding angle [36]
3. Roll off angle [31]
4. Coefficient of friction [38]
5. Static contact angle [33]

Chapter Summary

Superhydrophobic material possesses self-cleaning property which interests researchers the most. With SH coating, dust could be flushed away by rain and adhesion of dust could be reduced due to low surface energy of SH surface. To achieve superhydrophobicity, trapped air pockets between surface feature and water droplet should be stable. So water droplet can move freely on the SH surface and Cassie-Baxter equation could be used to describe the water contact angle behavior. However, CB state is a metastable stage so that if exterior force comes in, wetting behavior of water droplet would be driven to Wenzel state which is the stable state. Energy barrier of CB-Wenzel transition was also introduced and this equation tells that in order to stabilize CB state, surface energy should as small as possible and surface roughness factor should be as high as possible. With this perspective, SH materials have been fabricated in plenty of approaches such as moulding or photolithography. Nevertheless, current adversity for

application of SH material is durability. Several papers claimed they made durable SH surface but the durability test is not standardized and controversial.

CHAPTER 2
FABRICATION OF DURABLE AND SUPERHYDROPHOBIC PAINT WITH COMMERCIAL FLUORO POLYMER

Introduction

Several superhydrophobic surfaces are observed in nature, but their structures are also vulnerable to mechanical shear forces. Why, then, could they always possess superhydrophobic properties? The answer is regeneration. Artificial material is not able to regenerate surface structure like nature's creatures do. However, the concept of sacrificing layers is similar to regeneration. More specifically, a coating which can regenerate the rough surface and still possess the superhydrophobicity after wear is our core objective. Once the top layer of particles or nanofibers is removed, a second layer reveals the surface is still rough enough to show superhydrophobicity until whole coating is wiped out. One paint manufacturing company also disclosed some patents and named this design "volumetric SH coating,"[24]. In Chapter 2, the Lumiflon 4400 was chosen as the binder to form a polymer matrix, and the pigment was fumed silica. Silica carries the most sufficient hydroxyl group for the surface comparing to other ceramic particles, and a hydroxyl group is crucial for further silane bonding, such as perfluoro trichlorosilane or aliphatic alkyl silane. The density of the hydroxyl group strongly influences the ultimate silane density from which the hydrophobicity of particles come. Fluorinated silica particles were mixed with Lumiflon 4400 fluoropolymer in differing volume percentages. Threshold value to achieve superhydrophobicity is reported. Wettability change against wear, wear resistance and coating depletion rate (CDR) are also reported.

Standardize Wear Resistance Test for Superhydrophobic Coating/ Material

Although plenty of papers have announced durable superhydrophobic coating have been demonstrated already[36], [42]–[50]. The testing methods are not unified and standardized, which are listed in the Table 1-1. Therefore, ASTM D4060-14 [51] and ISO 7784-2 are

referenced as guidelines to quantify the durability of superhydrophobic materials. These two standards demonstrate a sound process to evaluate the wear resistance of test specimen.

The terminologies to express abrasion resistance listed in ASTM D4060-14 are:

- *Wear index, n*-1000 times the loss in weight in milligrams per cycle
- *Weight loss, n*-the loss in weight in milligrams, determined at a specified number of cycles.
- *Wear cycles per mil*, n-the number of cycles of abrasion required to wear a film through to the substrate per mil (0.001 in.) of film thickness.

The experimental process is summarized here:

An organic based coating with a certain thickness is attached to a rigid panel and abraded by rotary rubbing action under controlled loading and environment. Abrasion resistance is calculated as loss in weight after a specified number of abrasion cycles, as loss in weight per cycle, or as number of cycles required to remove a unit amount of coating thickness. ASTM D4060 records some conditions needed to be presented in the report, which are:

- 1. Temperature and humidity conditions during and at the time of testing
- 2. Thickness of coating when wear cycles are specified
- 3. Type of abrasive wheels used
- 4. Load applied to the abrasive wheels
- 5. Number of wear cycles recorded for each test specimen
- 6. Wear index, wear loss, or wear cycles per mile for each test specimen

Given the required properties of SH surfaces, which are 1) Static contact angle is over 150° and 2) Sliding or roll- off angle is smaller than 10 °, two measurements are proposed to classify the wear resistance of superhydrophobic material.

Measurement of Water Contact Angle Change against Abrasion Cycles

A wear resistance test should include the contact angle and sliding angle change compared to wiping cycle's increment. Simultaneously, type of abrasive and loading information should be reported as well. For example, silicon carbide sand papers with different

grits result in different friction behavior. Other conditions such as temperature, coating thickness, loading, and type of abrasive are also needed to be reported. With this information, researchers are able to understand the critical point where coatings lose superhydrophobicity.

Measurement of Weight Loss against Abrasion Cycles

Weight loss could be used to calculate the wear index and wear loss. This value could help researchers to evaluate how fast the coating degrades under abrasion. The weight of a sample is measured every 200 cycles with accuracy of ±0.1 mg. Afterwards, the data points could be fit in linear regression and the slope can be obtained, which could be defined as coating depletion rate (CDR). Other conditions, such as temperature, coating thickness, loading, and type of abrasive, need to be reported.

Novel Design Perspective of Durable Superhydrophobic Coating

Figure 2-1 illustrates the reason why traditional design of SH fabrication is fragile. After abrasion, the top of the structure is damaged, and two situations would occur. First, if the surface feature is made of intrinsic hydrophobic material such as polytetrafluoroethylene (PTFE), polydimethylsiloxane (PDMS), polystyrene (PS) etc, loss of surface roughness causes contact angle to decrease sharply and triggers CB state – Wenzel state transition. So, superhydrophobicity vanishes. If surface features are intrinsic hydrophilic they can still be hydrophobized by perfluoro silane or aliphatic silane. However, once the surface is damaged, the new surface will become hydrophilic. Hence, although the surface features are strong, minor surface damage influences the wettability. In this dissertation, a new perspective will be brought in to solve this disadvantage. Figure 2-1 B illustrates how this new design works; the white circles are hydrophobized metal oxide particles or nanofibers, and the yellow substrate represents the polymer matrix. After drying, the whole coating can be considered a particle-polymer composite material with thickness L and weight W. After abrasion, the top layer of the coating is

removed, and middle layer particles ascend to the surface, with retention of a random rough surface. Therefore, wettability could remain unchanged as long as the coating is not totally wiped off. After certain abrasion cycles, coating thickness drops to L' and weight changes to W'. By measuring the L' and W', ΔL and ΔW are obtained. The trend of ΔW is defined as coating depletion rate (CDR). Researchers can use this quantified data to understand the durability of coating and evaluate the strength of coating.

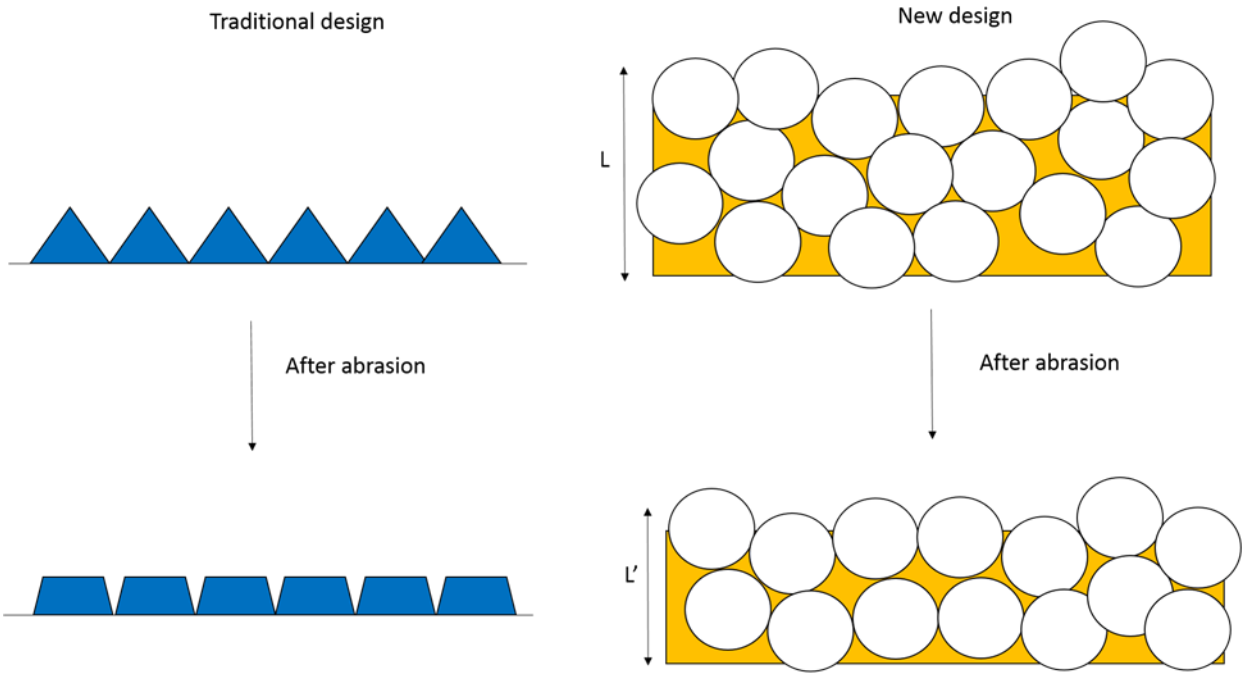

Figure 2-1. Difference of traditional design and new design. A) Traditional one layer design after abrasion B) Multilayer design after abrasion

Stacking of Granular Material

Gabrieli et al [52] elucidated the behavior of partially water saturated solid granules and divided them into five stages, shown in Figure 2-2. At the solid volume percent 100%, particles stack together without any water content. Packing density of particles are in the range of 56%~ 64%, which is also the empirical result of random closed packing. As the increase of liquid

portion, final structure transfers from dry to saturated stage. In pendular stage, particle grain is connected by little polymer and this polymer forms so called capillary bridge or pendular ring. In funicular state, pendular rings collapse and shared by more solid grains instead of connecting only between two solid grains. In capillary state, polymer domain is major rather than air domain. Therefore, Strength of final structure goes up with lower particle percentage but wall roughness of final structure decreases. To achieve durable superhydrophobic coating, both wettability and durability should be considered in the same time. However, final dried material with higher particle portion yields higher wall roughness but weaker structure. A criterion that provides enough wall roughness to achieve superhydrophobicity and possess decent strength, should be demonstrated.

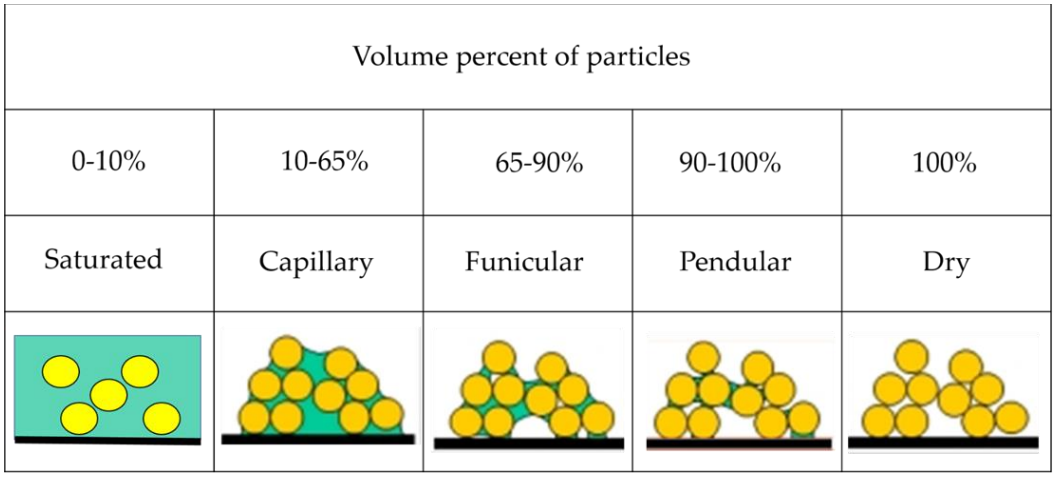

Figure 2-2. Schematic of final dried material with different particle-polymer ratio

Particles and Polymer Selection

Again, both chemistry and roughness determine the final wetting behavior of the surface. Submicron nanoparticles or nano rods could be used as a surface roughness contributor after being hydrophobized by our new design. Polymer binder selection is also significant here and is confined to intrinsic hydrophobic material category. Lumiflon 4400 is a water-borne fluoro polymer and possess 100° initial contact angle. Figure 2-2 shows the chemical structure of

Lumiflon 4400, which consists of tri fluoro units and hydrophilic functional groups. With sufficient fluoro units, Lumiflon 4400 is an intrinsically hydrophobic polymer and fulfills our demand.

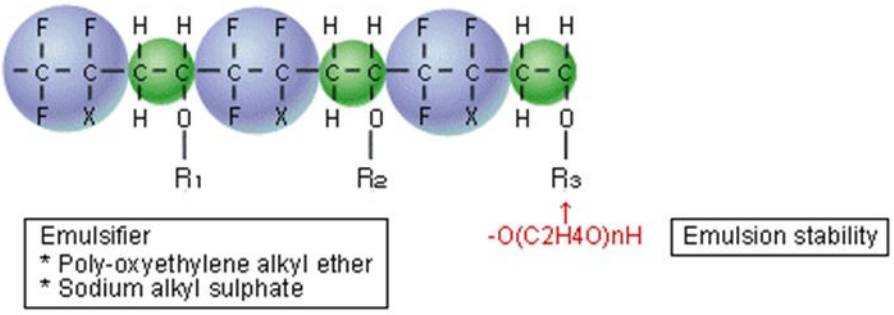

Figure 2-3. Chemical structure of Lumiflon 4400 from Asahi

Fabrication of Water Borne Superhydrophobic and Durable Coating with Commercial Fluoro Polymer

Materials and Experimental Process

Fabrication of superhydrophobic white pigments

Silica particles were purchased from Evonik Industries with the product name Aerosil Ox 50. The specific surface area is 35-65 m^2/ g. The processing starts with silica particles being dehydrated in the oven at 120°C and then dispersed in chloroform. Subsequently, heptadecafluoro-1, 1, 2, 2,-tetrahydrodecyltrichlorosilane, which is from Gelest Inc., was added to the silica-chloroform dispersion with the ratio 1ml: 1g silica and treated for 1 hour. Afterward, centrifuging the dispersion and decanting the chloroform follows. Drying of particles is done at 120C° on a heating plate for 5 hours. The fluorinated silica particles are obtained in this way.

Preparation of coating samples with different V%

These silica particles were combined in different proportions with Lumiflon FE-4400, a commercial water-based fluoropolymer resin emulsion used to produce coatings with high gloss and increased weatherability. Based on volume percent calculations, solutions ratios of

fluorinated silica to Lumiflon of 55V%, 60V%, 65V%, and 75V% were mixed. Additionally, ethanol was added as a solvent to help disperse the particles and aid in faster drying. These solutions were mixed using a vortex mixture, as well as with magnetic stirring bars for at least 6 hours.

Sample preparation

Soda-lime glass slides of 1"x1.5" were cleaned by isopropanol and left to dry in air for a minimum of 10 hours.

Method of measurement

Contact angle measurements were taken from high resolution photos of 30 μL DI water droplets by using Image J.

Durability testing was performed using a Taber 5700 linear abrader and 1200C grit silicon carbide metallurgical paper, manufactured by ALLIED high tech products Inc.

The loading pressure was 0.98N, and the wear index was also calculated from weight loss after every 200 cycles, up to 1000 cycles. (Definition of wear index is from ASTM D4060 – 14.)

Weight loss measurements were obtained by a TR104 Denver Instrument scale with an accuracy of 0.1mg.

Results and Discussion

Initial Contact Angle of White Coating with Different V% Pigments Adding

In Figure 2-4, ratio of fluorinated fumed silica was adjusted from 55V% to 75V%. In our expectation, higher volume percent of pigments in the whole coating should cause higher contact angle and better wettability. From equation 1-10, higher roughness should stabilize water droplet in Cassie-baxter state. Therefore, the contact angle increasing trend could be understood. Furthermore, Figure 2-4 illustrates how polymer distributed in particles-polymer composite. Volume percent of polymer decreases from left to right and expresses different distribution

status. Because of surface tension and capillary force, polymer tends to adhere on the surface of particles and pores would be created in the polymer matrix. This is also called funicular stage. With increasing in particle ratio, polymer bridge forms and chains each particles together. Therefore, higher V% of adding pigments leads to polymer distribution stage shifting from saturated to pendular and enhances surface roughness factor.

Solution Recipe	Initial DI Water Contact Angle
55V% of fluorinated silica to Lumiflon 4400	152 ± 2° 
60V% of fluorinated silica to Lumiflon 4400	152 ± 2° 
65V% of fluorinated silica to Lumiflon 4400	154 ± 2° 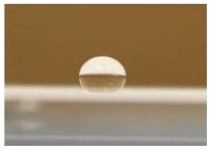
75V% of fluorinated silica to Lumiflon 4400	156 ± 2° 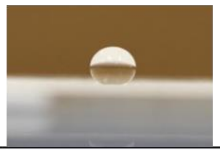

Figure 2-4. Higher volume percent of fluorinated silica adding turns out higher initial contact angle

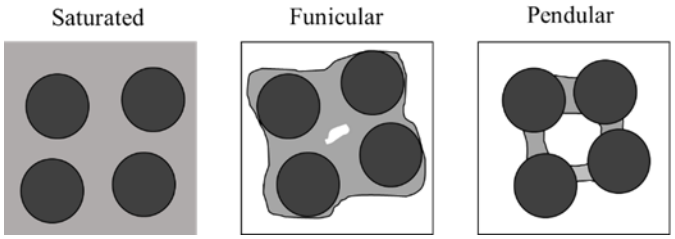

Figure 2-5. Scheme of polymer distribution status with different volume percent in particle-binder composite

Abrasion Test with 1200P Sandpaper as Abrader - Lumiflon White Paint System

Abrasion test was operated by Taber linear abraser and loading was 0.98N and contact angle and weight were measured every 200 cycles. Contact angle change and weight change are listed in the Figure 2-5 and Figure 2-6. In Figure 2-5, 75V% sample, which possesses the weakest structure, was wiped out before 400 cycles so only two points were shown. 65V% sample was also demolished before 600cycles. Trade-off occurs between wear resistance and wettability. 60V% sample survived after 1000 times abrasion by 1200C sand paper. Contact angle was around 151°±2° after 1000 time abrasion. However, contact angle of 55V% sample was dropping gradually with abrasion cycles increasing. The reason is that structure of 55V% is stronger than 60V% so that polymer matrix of 55V% was not damaged by 1200C sand paper which means only particles on the top layer were removed. In doing this, a new layer of particles can't ascend to top layer to provide new rough surface so contact angle declined and reached intrinsic contact angle of Lumiflon resin eventually which is around 120°

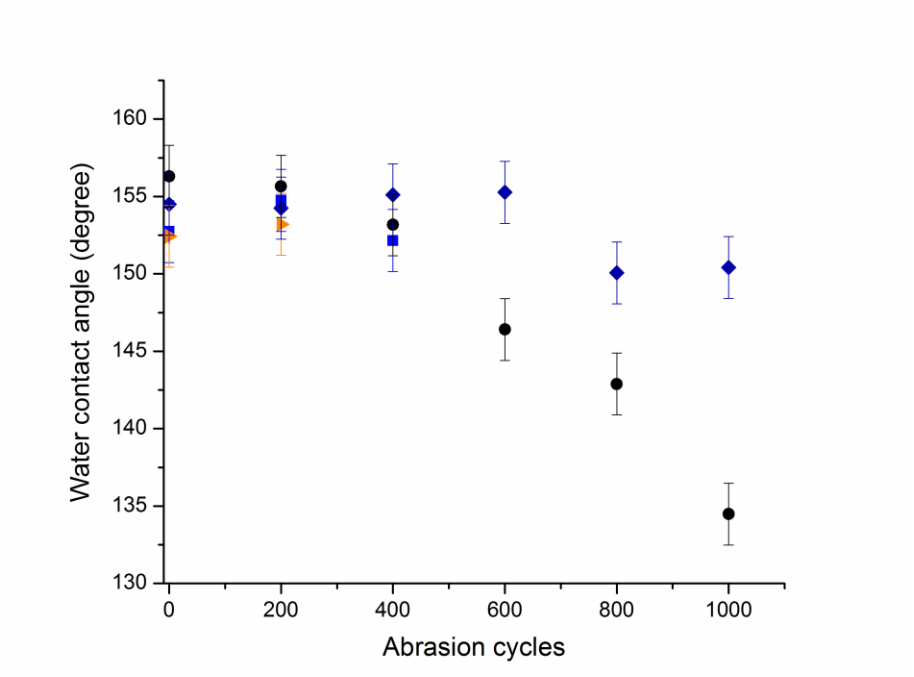

Figure 2-6. Water contact angle change against abrasion cycles – Lumiflon white paint system (▶: 75V%, ■: 65V%, ♦: 60 V%, ●: 55V %)

CDR of 75V% sample was the highest and reached 100% loss before 400 cycles and 65V% loss 100% before 600 cycles. Interestingly, 60V% and 55V% lost around 16% and it may not be wiped out until 10,000 cycles.

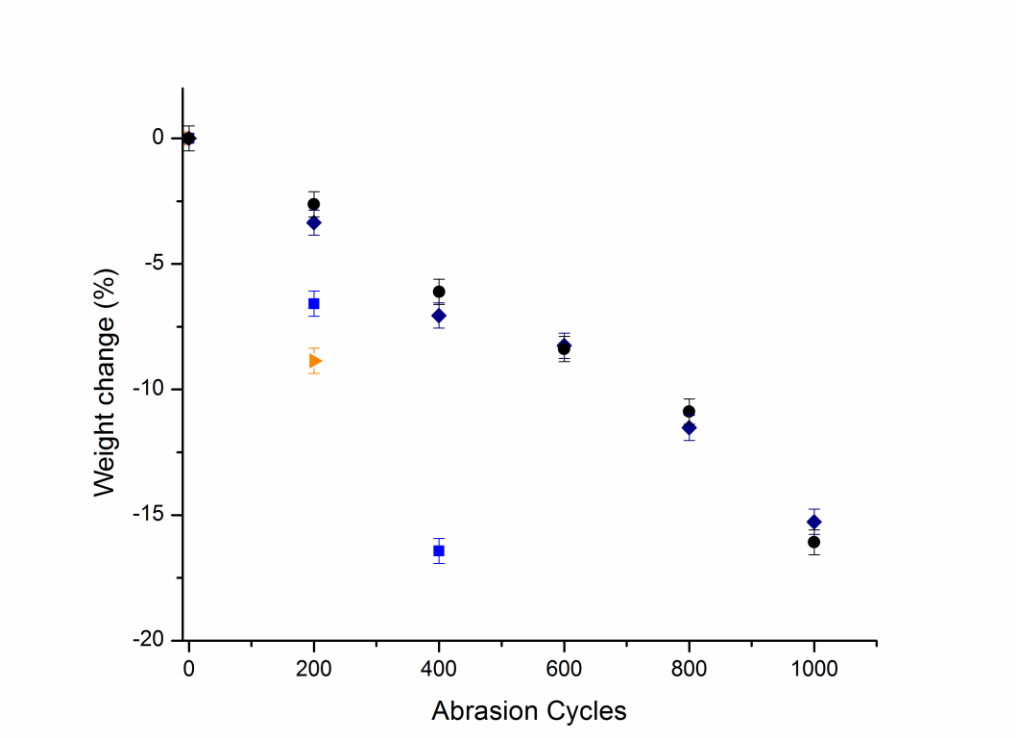

Figure 2-7. Weight change against abrasion cycles – Lumiflon white paint system (▶: 75V%, ■: 65V%, ♦: 60 V%, ●: 55V %)

Combine the result in Figure 2-6 and Figure 2-7, particle volume percent 55V% to 60V% is preferable to make durable superhydrophobic coating.

Summary

In Chapter 2, new perspective of superhydrophobic material was introduced. Unlike the traditional one-layered surface feature, new design used multi-layered structure to overcome durability issue in old design. The idea is that once top layer of coating is removed, new layer of particle reveals itself and provides roughness so that coating can possess superhydrophobicity until whole coating is destroyed. Moreover, durable superhydrophobic white paint was successfully made of fluorinated silica particles and commercial fluoropolymer. By varying the

volume percent of pigment, 55V% to 60V% was found to be the critical range in which coating was still in superhydrophic regime after 1000 times of abrasion with a loading of 0.98N. This is the first report with quantitative wear resistance of superhydrophobic material. Also, first superhydrophobic coating that could be worn 1000 times by sand paper was illustrated and this result has been patented.

CHAPTER 3
FABRICATION OF DURABLE AND SUPERHYDROPHOBIC COLOR PAINTS

Introduction

In Chapter 2, a durable superhydrophobic white coating was made successfully, and changing the traditional superhydrophobic one layer surface feature to a multilayer structure was demonstrated. In Chapter 3, we follow this core perspective and reduce dependence on commercial products. PVDF-PMMA mixed polymer was chosen to be the main components of the polymer matrix. In the first part, white paints were made with different volume percent of pigment; wettability, contact angle change with abrasion and coating depletion rate (CDR) were reported. To improve the applicability of these superhydrophobic coatings, black, blue, red, and green superhydrophobic coatings were created as well. Most natural color mattes are metal oxide compounds; metal oxides have abundant hydroxyl groups on the surface where the surface modifier aims to bond. For example, ultramarine is a common blue matte, iron oxide can be used to make red and black paints, and chromium oxide is for green paint fabrication. After fluorination, these color mattes can be used to fabricate superhydrophobic color paint. Although only 5 different colors of paints were reported in this dissertation, other colored superhydrophobic paints could be achieved by this approach as well. In Chapter 2, white superhydrophobic paint was created with different volume percent of pigment. The results show that a higher volume percent of pigment yields higher roughness because the polymer matrix distribution shifts. In Chapter 3, V% is still the parameter, and thresholds of V% to achieve superhydrophobicity (CA> 150°) were all found in the range of 60V% to 70V% for different colors of paint. This point is the transition point from capillary state to funicular state and also the highest possible packing density of random close packing. This range could be used a general principle to fabricate durable and superhydrophobic volumetric coatings

Superhydrophobic White Paint Fabrication and Characterization

Materials and Experimental Process

Fabrication of superhydrophobic white pigments

Aerosil Ox 50 Silica particles were purchased from Evonik Industries; the specific surface area is 35-65 m^2/g. Processing of these particles was achieved by dehydrating the silica particles in the oven at 120°C and dispersing them in chloroform. Subsequently, heptadecafluoro-1, 1, 2, 2,-tetrahydrodecyltrichlorosilcane, from Gelest Inc., was added to the silica-chloroform dispersion with the ratio 1ml: 1g silica and treated for 1h. The dispersion was then centrifuged; decanting of the chloroform followed dispersion. The particles were dried at 120°C on a heating plate for 5hs, yielding the desired fluorinated silica particles.

Binder blending

The PVDF source was Kynar Hsv 900 with a molecular weight of 900,000-1,300,000 g/mol. The PMMA used, from Polyscience Inc., was a blend of: 3.96g DMF, 0.21g PVDF, 0.8g acetone, 0.04g PMMA, 1g triethyl phosphate, and 100 µl perfluoro compound F-75C (purchased from ACROS). A vortex mixer was then used to homogenize the liquid part of paint. This solution is considered the "standard binder solution" (SBS), and is discussed in the following paragraphs.

Preparation of coating samples with different V%

After blending the binder, fluorinated silica particles were added at different volume percent: 65.22% (with 0.6g fluorinated silica particles added), 61.08% (with 0.5g fluorinated silica particles added), 55.85% (with 0.4g fluorinated silica particles added), 48.57% (with 0.2g fluorinated silica particles added) and 38.46% (with 0.2g fluorinated silica particles added). After vigorous stirring for 6 hours, 1"x 1.5" soda-lime glass slides were coated and spun at 100 rpm by a spin coater. The slides were dried in air for at least 10 hours.

Method used for measurement

Contact angle measurements were taken from high resolution photos of 15 µL DI water droplets using Image J. Durability testing was performed using a Taber 5700 linear abrader and 1200P grit silicon carbide metallurgical paper, manufactured by ALLIED high tech products Inc. The loading pressure was 0.98N, calculated out to be about 50 kPa, and the wear index was also calculated from weight loss after every 200 cycles, up to 1000 cycles. (Definition of wear index is from ASTM D4060 – 14.) Weight loss measurements were obtained by a TR104 Denver Instrument scale with an accuracy of 0.1mg

Results and Discussion

Initial Contact Angle Measurement

Coatings with different pigment volume percent yield different initial WCA, and the results are shown in Figure 3-1. Obviously, coating with a higher V% will have a higher initial WCA. According to the Cassie-Baxter model, the contact angle depends on the fraction of contact material, which means that the rougher the surface is, the higher the WCA the material possesses. Interestingly, there is a sharp increase in contact angle between paint with 55.85V% and paint with 61.08V%.

Recipe	Initial Water Contact Angle
0.6g pigments adding (Volume % of pigment: 65.22%)	158±2° 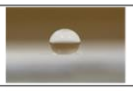
0.5g pigments adding (Volume % of pigment: 61.08%)	155±2° 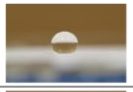
0.4g pigments adding (Volume % of pigment: 55.85%)	152±2° 
0.3g pigments adding (Volume % of pigment: 48.57%)	151±2° 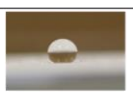
0.2g pigments adding (Volume % of pigment: 38.46%)	140±2° 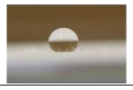

Figure 3-1. Higher pigment V% yields higher initial contact angle - white paint

Contact Angle Change with Abrasion Test

Figure 3-2 shows how contact angle decreases with increasing number of wiping cycles by various V% of pigments. In terms of our volumetric system design, once the top layer is removed, the second layer is revealed and still possesses superhydrophobicity until whole layer coating is wiped off. Basically, five samples still have the trend of decreasing contact angles; however, 65.22V% and 61.08V% are still above 150° after 1000 abrasion cycles. Moreover, although the CA of the 55.85V% sample drops below 150° after 1000 abrasion cycles, it possesses 147° contact angle, which is close to SH regime. This shows that lower V% samples, e.g. 38.46V% and 48.57% and 55.85%, degrade much slower than the paint with higher V% because the particles embedded in the binder matrix in the lower V% coating were in a saturated status. The scheme of polymer distribution changes with the polymer volume percent as shown in Figure 3-4. In contrast, paint samples with higher V% suffered obvious contact angle decrease at beginning, but the trend gradually slowed.

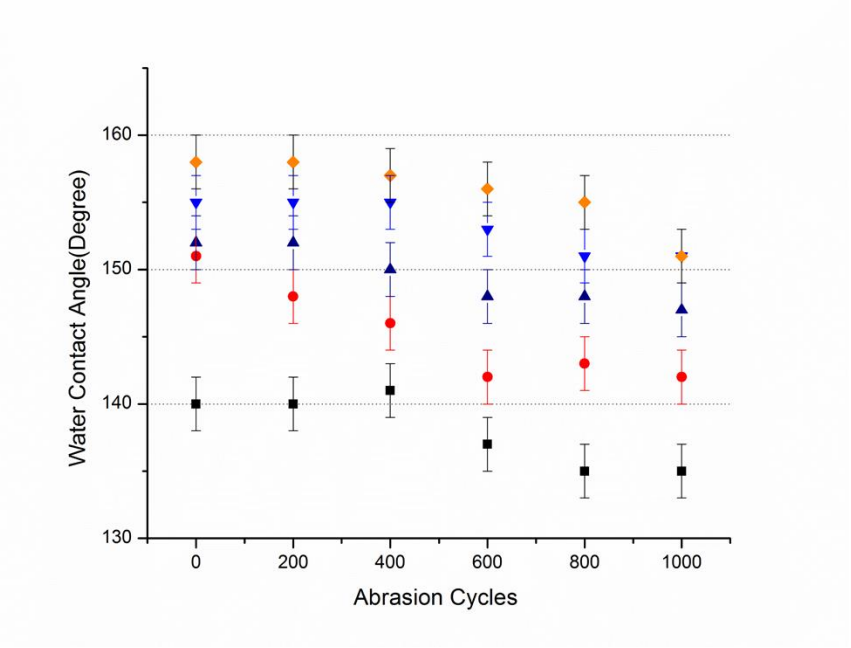

Figure 3-2. Contact angle decreases with abrasion cycles increase- white paint (♦: 65.22V%, ▼: 61.08 V%, ▲: 55.85V%, ●: 48.57 V%, ■: 38.46 V %)

Sample V%	■:38.46 V%	●: 48.57 V%	▲:55.85V%	▼:61.08V%	♦:65.22V%
Slope of regression line of contact angle change	-6.3E-3	-9.1 E-3	-5.6 E-3	-6.2 E-3	-5.5 E-3

Figure 3-3. List of slopes of the regression line of decreasing WCA-white paint system

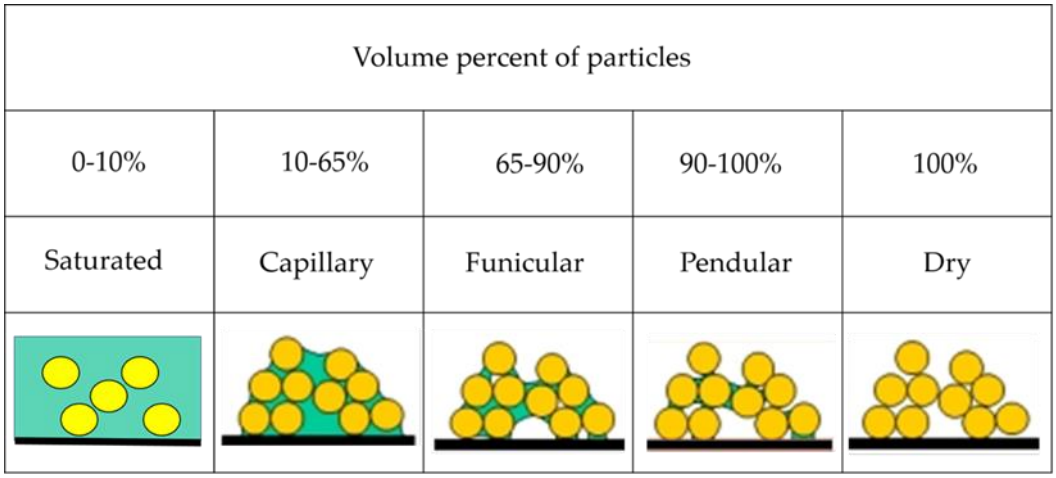

Figure 3-4. Scheme of polymer distribution status with different volume percent in particle-binder composite

Wear Index and CDR Calculation

The definition of wear index is n-1000 times the loss in weight, in milligram per cycle, which is from ASTM D4060 – 14. Figure 3-5 shows weight loss of testing samples and Figure 3-6 lists the wear index corresponding to different V%. As the results show, 38.46V%, 48.57V% and 55.85V% have similar wear resistance and weight loss after 1000 abrasion cycles, around 5~6%. However, there is a jump between 61.08% and 55.85% because the binder distribution status changes from capillary stage to funicular stage (shown in Figure 3-4), so that the weight loss of 61.08V% and 65.22% is larger than the lower V% coatings. In summary, the weight loss of the 5 samples after 1000 abrasion cycles is less than 15%. Interestingly, the random close-packing density for slow settlement is 56%, which could be used to explain why we obtained two different coating depleting rates (CDR). Coating with V% lower than 56% show a thin film

structure and possess a lower CDR. After the V% is over 56%, the polymer distribution becomes funicular or even pendular, making the structure less rigid.

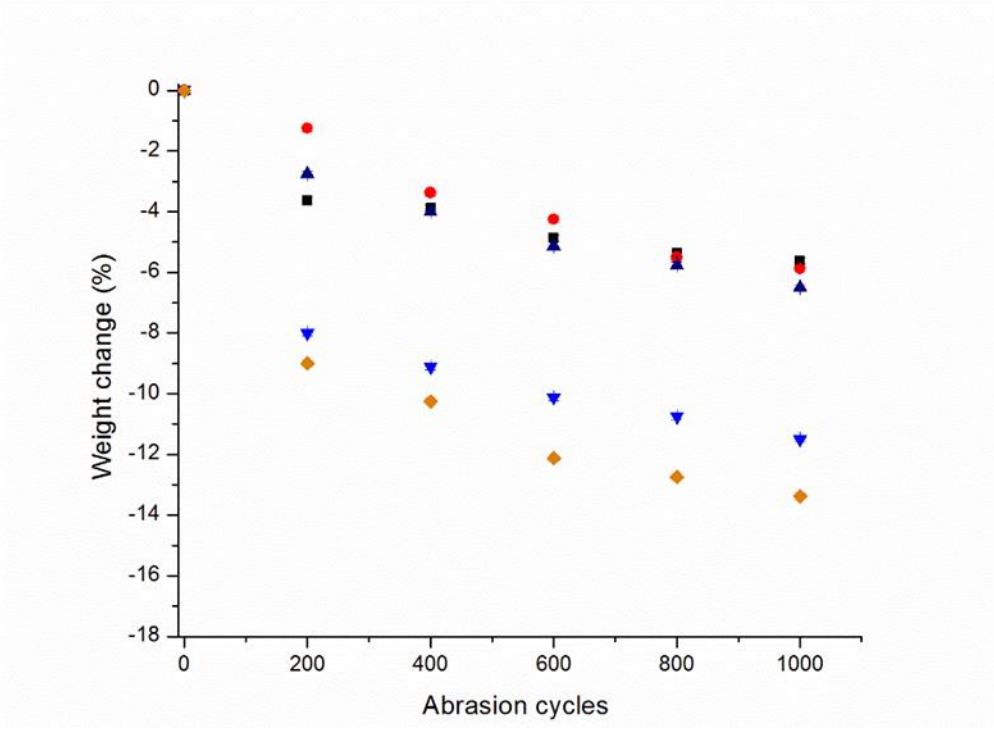

Figure 3-5. Weight loss with different volume percent after abrasion- white paint (♦: 65.22V%, ▼: 61.08 V%, ▲: 55.85V%, ●: 48.57 V%, ■: 38.46 V %)

Sample V%	■:38.46 V%	●: 48.57 V%	▲:55.85V%	▼:61.08V%	♦:65.22V%
Wear Index (mg/cycle)	-4.5×10^{-3}	-4.7×10^{-3}	-5.2×10^{-3}	-9.2×10^{-3}	-10.7×10^{-3}
Percentage of weight change to initial weight after 1000 cycles abrasion (%)	5.62± 0.5%	5.87± 0.5%	6.5± 0.5%	11.5± 0.5%	13.38± 0.5%
Slope of regression line (CDR)	-4.91E-3	-6.14 E-3	-6.09 E-3	-9.54 E-3	11.43 E-3

Figure 3-6. List of wear index, weight loss part per thousand, and slope of regression line for by varying the Volume percent of pigments adding

SEM Characterization

Figure 3-7 to Figure 3-10 show SEM images of the cross-section of the paints with 38.46V%, 55.85V%, 61.08V% and 65.22B% in sequence. The white circles indicate an enlarged

area for the image in higher magnification. In Figure 3-7, the final dried material forms a thin-film like structure because the polymer distribution is in capillary state (shown in Figure 2-2) and hydrophobized particles were surrounded by the polymer domain. Therefore, in this situation, lower roughness surface results in a lower initial contact angle(only 140°) but lower coating depletion rate (CDR), which means a more rigid structure.

Figure 3-8 and Figure 3-9 show the cross section images of coating with 55.85V% and 61.08V%. Higher paritlce volume percent turns out a rougher surface and higher initial contact angle.

Ultimately, the 65.22V% coating, which is shown in Figure 3-10, reveals a distinctly different structure in Figure 3-7. Evident from the image, the structure has much rougher surface than image in Figure 3-7. The polymer distribution status is in the funicular state and formed flaky structure. This the reason why 65.22V% could possess 160° WCA. Although this film's depleting trend is faster than the coating with lower V%, the 65.22V% coating is still superhydrophobic after 1000 abrasion cycles.

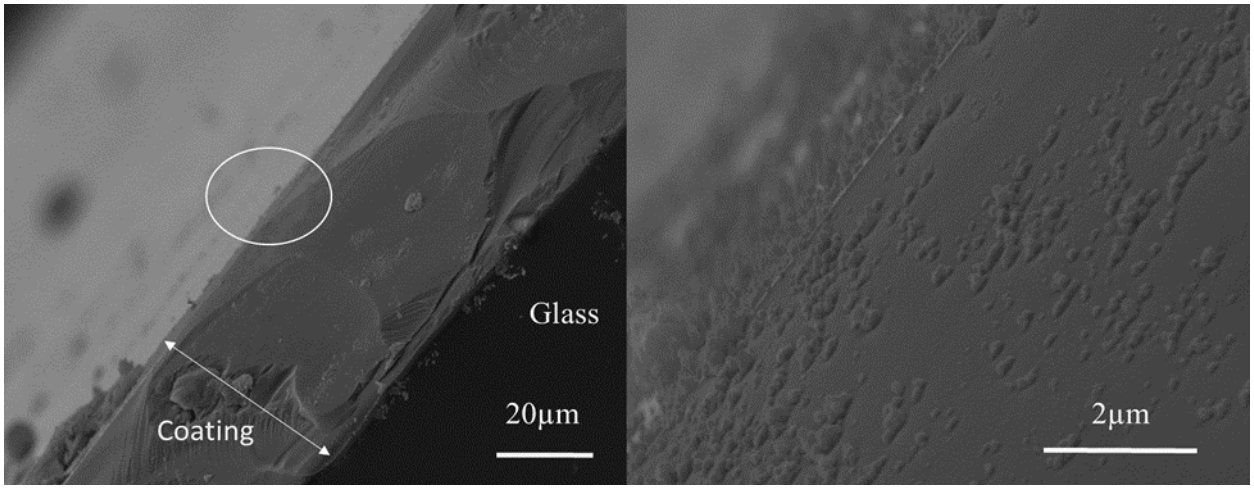

Figure 3-7. Cross-section of coating with 38.46V% of particle and the polymer distribution is in capillary stage. (Photo courtesy of author)

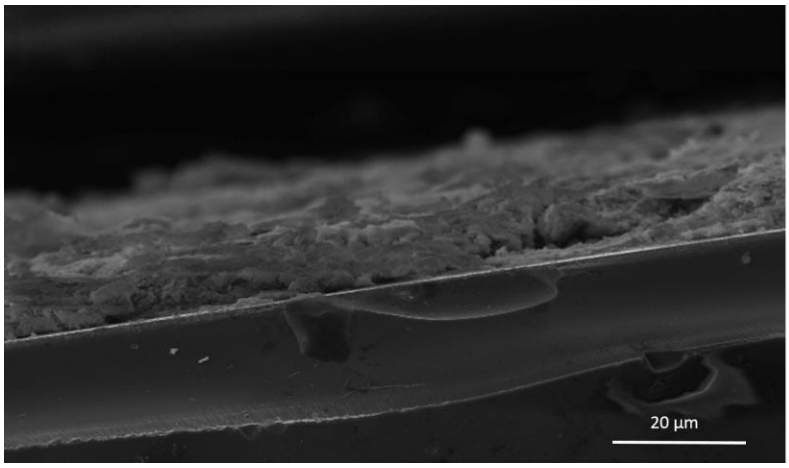

Figure 3-8. Cross-section of coating with 55.85V% of particle. (Photo courtesy of author)

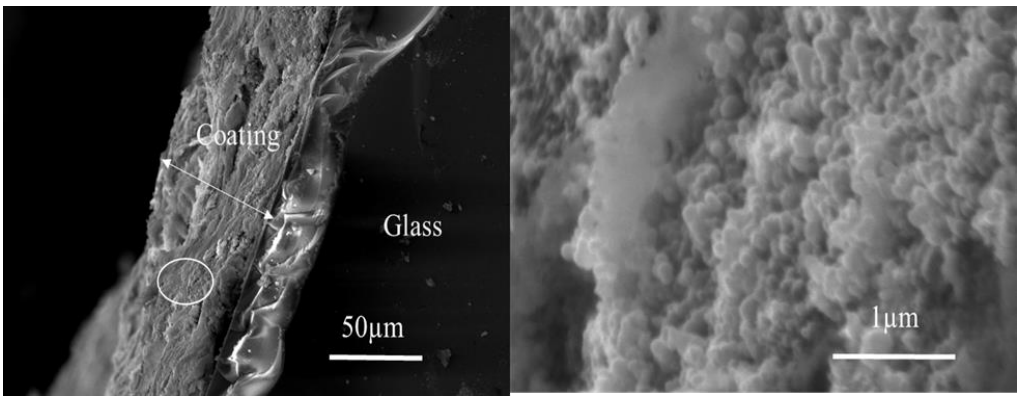

Figure 3-9. Cross-section of coating with 61.08V% paint and the polymer distribution is in funicular stage. (Photo courtesy of author)

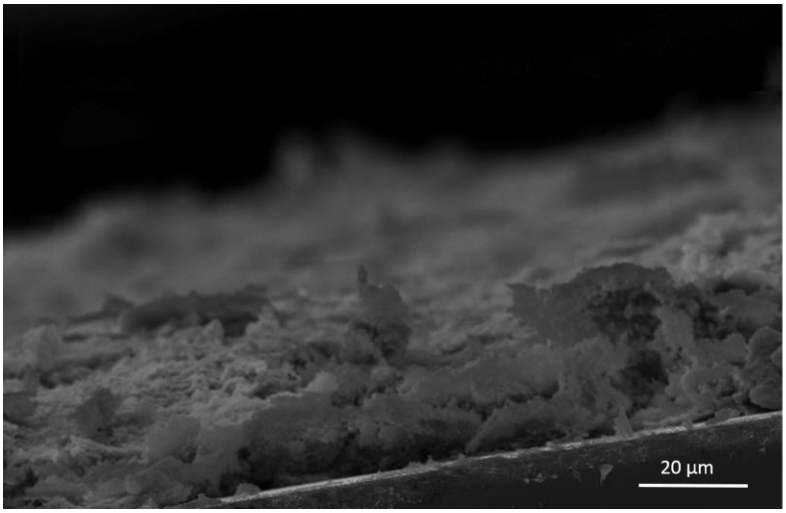

Figure 3-10. Cross-section of coating with 65.22V% paint and particles are bonded by polymer bridge and show a flaky structure. (Photo courtesy of author)

Discussion and Understanding

Based on the empirical statistic of random close packing, the possible packing density is in the range of 56% to 64% [53]–[57]. In order to understand the possible wall roughness of our final dried material, FCC (111) and simple cubic (100) were chosen to be the upper limit and lower limit. FCC (111) is the close packed plane, whose packing density is 74%, in FCC structure and the calculated roughness factor is 1.9 (shown in Figure 3-11). On the other hand, packing density of plane (100) in simple cubic structure is 52% and turns out roughness factor$r = 1.78$. In the white paint system, depend on the contact angle measurement (Figure 3-1) and equation 1-5, 1-8, 1-10, wall roughness of final dried material with varied particle volume percent were calculated and shown in Figure 3-12. Roughness factors of sample 55.8V%, 61.1V%, 65.2V% are in the range of 1.78-1.9, which is our expected range.

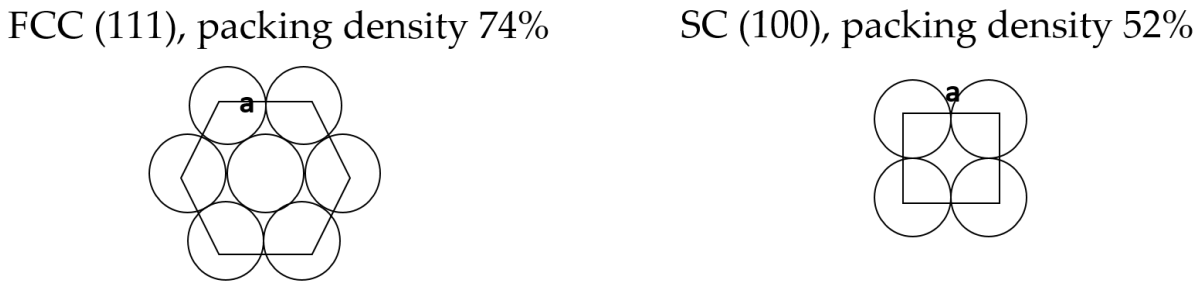

Figure 3-11. Calculated roughness factor (r) of surfaces with packing density 74% and 52%

Sample V%	■:38.5 V%	●: 48.6 V%	▲:55.8V%	▼:61.1V%	♦:65.2V%
Contact angle	θ_W:140°	θ_{CB}:151°	θ_{CB}:152°	θ_{CB}:155°	θ_{CB}: 158°
f_s (solid fraction)	Wenzel	0.25	0.23	0.19	0.14
r (roughness factor)	1.52	1.74	1.76	1.81	1.86

Figure 3-12. Calculated solid fraction (f_s) and roughness factor (r)

Threshold to achieve superhydrophobicity for white paint system is between 61% to 65V% and this value is close to the transition point of capillary structure to funicular structure. Hence, in order to fabricate the superhydrophobic coating with the highest mechanical durability, particle volume percent should be in the range of 60V% to 70V%.

Summary

This data is the first in the literature to quantify superhydrophobicity and its durability. Previous work that was reported by other groups only provided preliminary tests that are neither reproducible nor quantifiable. Baye et al trampled testing samples with their shoes and used this method to conclude durability of the coating. Although they mentioned human weight is 90 kg, they missed many parameters such as pressure, roughness, abrasive material (sand/dirt on shoe) and type of loading, i.e. tangential shear vs. torsion. In a report by Xiu et al [46], the sample was abraded for only one cycle and the applied force is not stated. Therefore, in this paper, we developed a wear resistance test based on similar ASTM tests for coatings. Our samples show quantifiable wear resistance and superhydrophobic properties after 1000 abrasion cycles. Wear index is reported to help researchers to evaluate the rigidity of the coating, which depends on the solid loading of pigments.

This work reports the first quantitatively tested superhydrophobic coating. Coatings have been made with various solid loadings of pigments. Superhydrophobicity was achieved for samples containing 65.2V% and 61.1V% of pigments. These coating showed superhydrophobicity after fabrication and continued to be superhydrophobic during the abrasion testing, well after 1000 abrasion cycles by metallurgy sand paper (1200C). The coating depletion +rate (CDR) is higher for a pendular structure of a coating and becomes less for denser structures. Despite the open pendular structure, the 65.2 V% has only losses of 15% from 1000 abrasion cycles. Both coatings could be painted on commercial products to provide

superhydrophobic properties, thus keeping the surfaces clean and dry. We expect that it extends enhanced anti-corrosion, anti-fouling properties, and more.

Superhydrophobic Black Paint Fabrication and Characterization

Materials and Experimental Process

Fabrication of superhydrophobic black pigments

Iron oxide black matte was purchased online from Powdered-Up Dolly. The processing starts with iron oxide particles being dehydrated in the oven at 120C°, which are then dispersed in chloroform. Subsequently, heptadecafluoro-1, 1, 2, 2,-tetrahydrodecyltrichlorosilcane, from Gelest Inc., was added to the iron oxide-chloroform dispersion with the ratio 1ml: 1g iron oxide and treated for 1 hour. Afterwards, the dispersion was centrifuged and the chloroform was decanted. Drying of particles was done at 120C° on a heating plate for 5 hours. The fluorinated black matte was obtained in this way.

Binder blending

Standard binder solution (SBS) was used for black paint fabrication, and the recipe is listed in white paint section.

Preparation of coating samples with different V%

To achieve black matte, fluorinated iron oxide was added to the SBS at different volume percent: 75% (with 2.26g fluorinated iron oxide added), 70% (with 1.78 fluorinated iron oxide added), 65% (with 1.45g fluorinated iron oxide added), and 60% (with 1.11g fluorinated iron oxide added). After vigorous stirring for 6 hours, 1”x 1.5” soda-lime glass slides were coated and spun at 100 rpm by a spin coater. The slides were dried in air for at least 24 hours.

Results and Discussion

Initial Contact Angle Measurement

In black paint system, the threshold to achieve superhydrophobicity was found between 60 V% to 65V% (shown in Figure 3-13), with contact angle increasing with more pigments added. Compared to threshold value of white paint, which is around 55%~60%, value of black paint is higher. The reason for this is that silica particles (white pigment) have more hydroxyl groups on the surface than that of the iron oxide particles (black pigment). This suggests that coverage of fluorosilane on silica is higher than on iron oxide, meaning that higher surface roughness is needed to achieve superhydrophobic regime in iron oxide system. Eq. 1.10 shows how a surface with a lower young's contact angle needs higher surface roughness (r) to stabilize a droplet to stay in Cassie-Baxter state. This equation explains why the threshold value of black paint is higher than white paint.

Recipe	Initial Water Contact Angle
2.26g pigments in SBS (Volume % of pigment: 75%)	155±2° 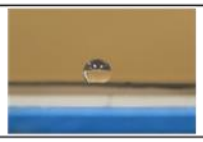
1.78g pigments in SBS (Volume % of pigment: 70%)	154±2° 
1.45g pigments in SBS (Volume % of pigment: 65%)	150±2° 
1.11g pigments in SBS (Volume % of pigment: 60%)	148±2° 

Figure 3-13. Initial contact angle of black paint with different V%- black paint

Black Paint Wear Resistance Test by Using 1200C Sand Paper as Abrader

Figure 3-14 shows how contact angle changes as abrasion cycles increase. Declining trends of the 75V% and 70V% paints are more obvious than that of the 65% and 60% paints. Because higher V% yields more fragile structure, the contact angle of these four samples dropped below 150° after 400 cycles.

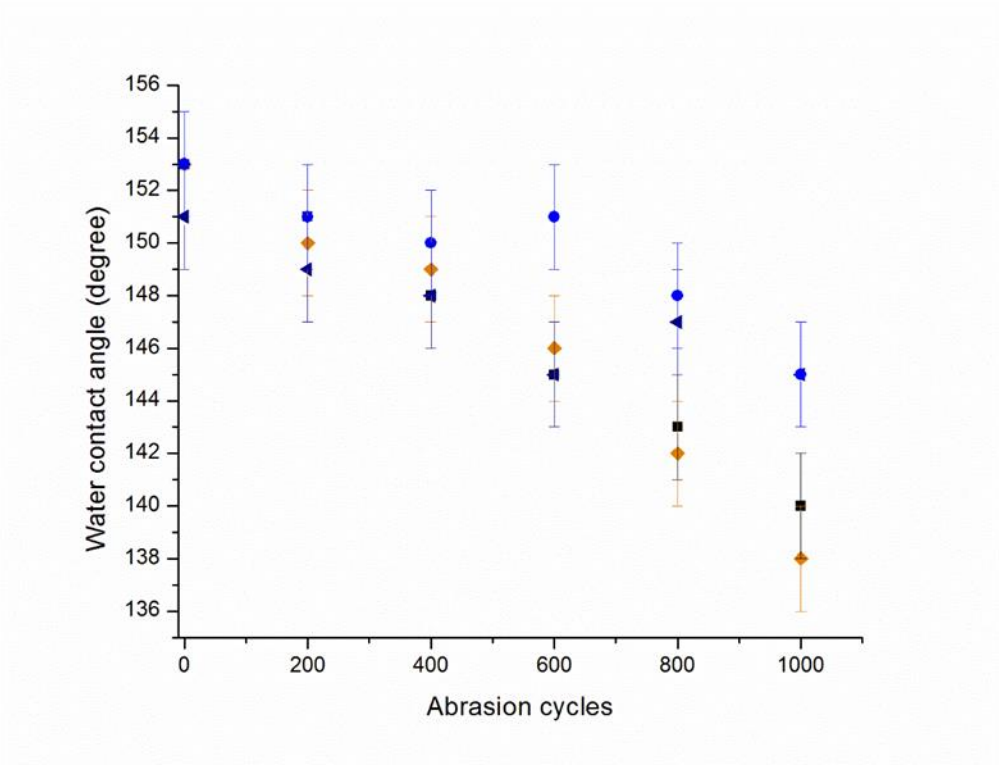

Figure 3-14. Contact angle changes against abrasion cycles increase - black paint/ 1200C sand paper (♦: 75V%, ■: 70V%, ►:65 V%, ●: 60 V %)

Sample V%	●: 60 V%	►:65 V%	■: 70 V%	♦: 75 V%
Slope of regression line of contact angle change	-6.86E-3	-5.57 E-3	-13.1E-3	-14.57E-3

Figure 3-15. List of contact angle trend - black paint/ 1200C sand paper

Figure 3-16 and Figure 3-17 exhibit weight loss (%) and CDR of black paint with different V%. Under abrasion of 1200C sand paper, weight loss and CDR of four samples were quite similar, which was around 5~6 %. Here, the explanation is that 1200C sand paper is too fine to destroy the polymer matrix so that only top layer of fluorinated iron oxide particles were removed. The retained polymer matrix was compressed by pressure from abrader loading (50 kPa). That is the reason why the contact angle kept declining and eventually reach the value that the pure PVDF-PMMA mixed polymer possesses (The contact angle of PVDF-PMMA mixed polymer is 100°).

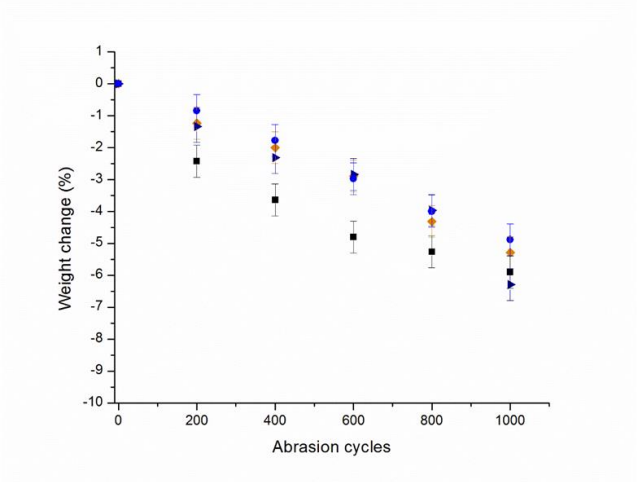

Figure 3-16. Weight loss with different volume percent after abrasion- black paint (♦: 75V%, ■: 70V%, ▶:65 V%, ●: 60 V %) - black paint/ 1200C sand paper

Sample V%	●: 60 V%	▶:65 V%	■: 70 V%	♦: 75 V%
Wear Index (mg/cycle)	-0.011	-0.012	-0.01	-0.014
Percentage of weight change to initial weight after 1000 cycles abrasion (%)	-4.55±0.5%	-6.29%±0.5%	-5.9%±0.5%	-5.28%±0.5%
Slope of regression line (CDR)	-5.01E-3	-5.7E-3	-5.6E-3	-5.22E-3

Figure 3-17. List of wear index, weight loss part per thousand, and slope of regression line for by varying the volume percent of pigments adding- black paint/ 1200C sand paper

Black Paint Wear Resistance Test by Using 600 C Sandpaper as Abrader

Results shown in the 1200 C sandpaper abrasion test don't match our core design perspective. Because 1200C sand paper only removed the top layer of particles but the polymer matrix is still sturdy. So, we chose 600C sand paper to be applied to black superhydrophobic abrasion test. Because 600C sand paper is rougher than 1200C, the goal of using 600C is to destroy polymer matrix layer by layer. With damaging of polymer matrix, we expect the contact angle should not change sharply but the CDR might be higher than the results abraded by 1200C. The outcomes shown in the Figure 3-18 and Figure 3-19 match our expectation. The contact angle after abrasion keeps fluctuating and the declining trend is close to zero. Rougher sand paper can destroy the polymer matrix so new layer of fluorinated particles unveil and random packaging of particles contributes high roughness. Thus, the contact angle remain stable in this abrasion test.

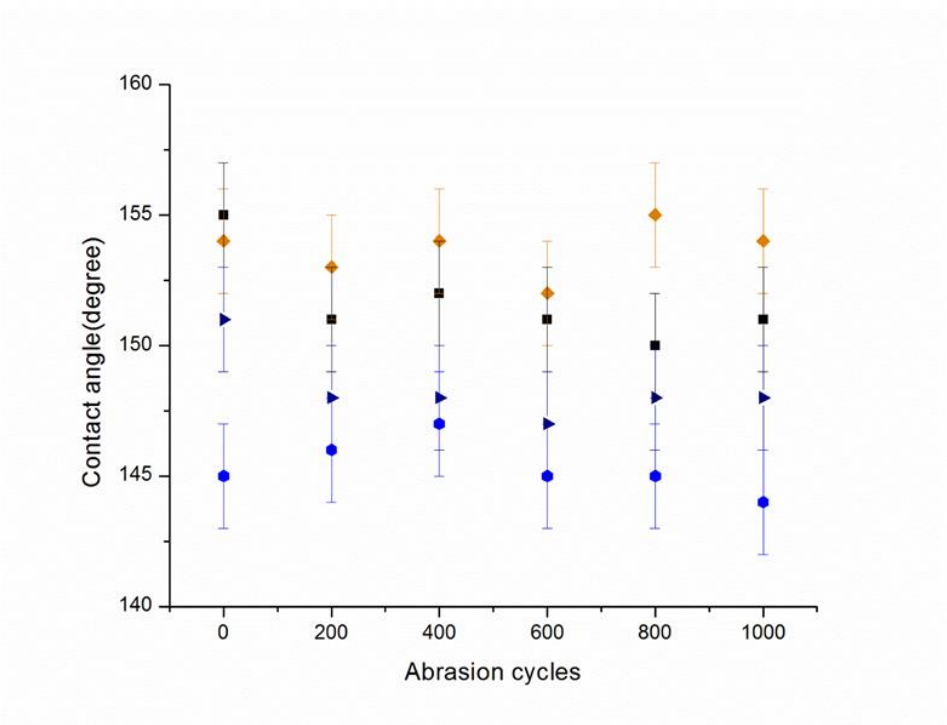

Figure 3-18. Contact angle fluctuate with abrasion cycles increase- black paint/ 600C sand paper (♦: 75V%, ■: 70V%, ►:65 V%, ●: 60 V %)

Sample V%	●: 60 V%	►:65 V%	■: 70 V%	♦: 75 V%
Slope of regression line of contact angle change	-1.43E-3	-2.29E-3	-3.43E-3	-5.71E-4

Figure 3-19. Contact angle declining trend -black paint / 600C sand paper

Figure 3-20 and Figure 3-21 list weight loss and CDR of black paint under 600C sand paper abrasion. Compare to the data under 1200C sand paper abrasion. Weight loss increases significantly with rougher sand paper. 75V% sample lost 31% of weight, 70V% sample lost 26% and this value is 500% ~600% comparing to the weight lost under 1200C abrasion. This data proves the explanation that polymer matrix damages or not strongly influences the wettability.

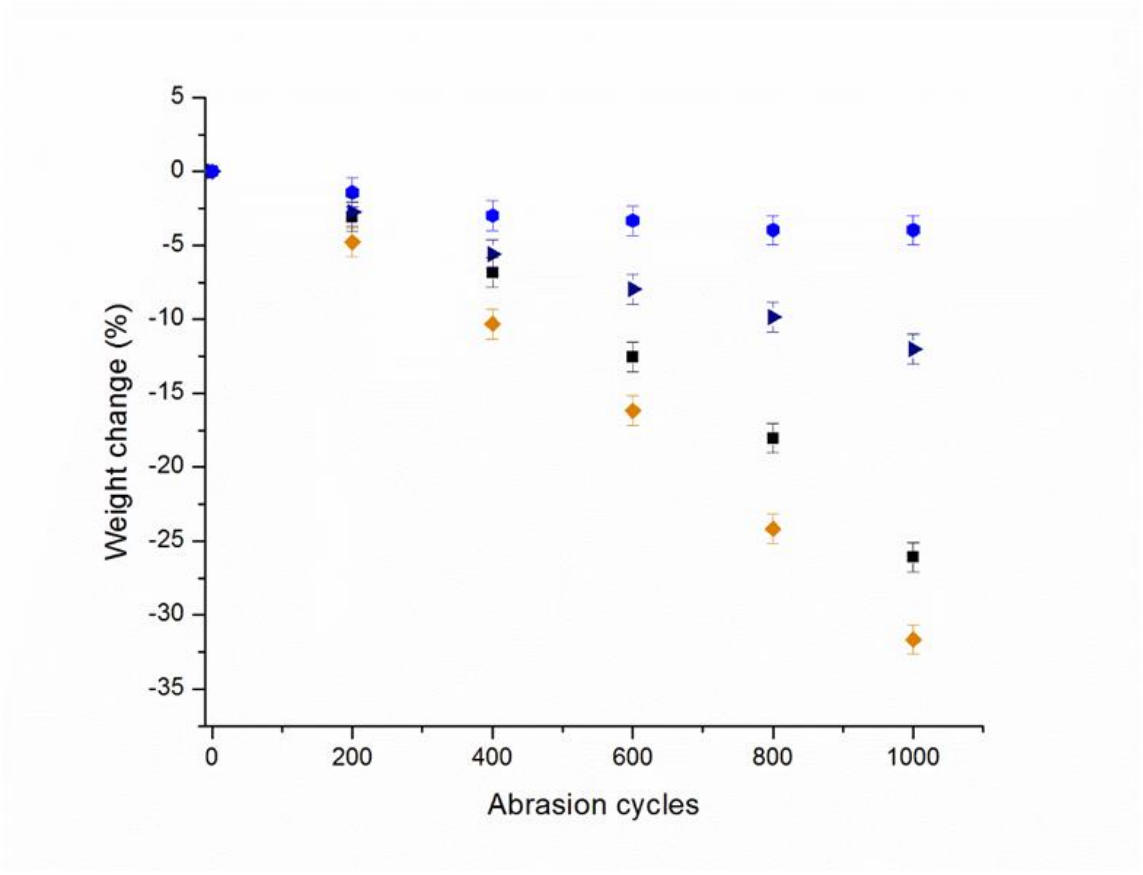

Figure 3-20. Weight loss with different volume percent after abrasion -black paint/ 600C sand paper (♦: 75V%, ■: 70V%, ►:65 V%, ●: 60 V %)

Sample V%	●: 60 V%	▶:65 V%	■: 70 V%	♦: 75 V%
Wear Index (mg/cycle)	-5.6 x10^{-3}	-0.02	-0.047	-0.089
Percentage of weight change to initial weight after 1000 cycles abrasion (%)	-3.96±0.5%	-12±0.5%	-26.08±0.5%	-31.66±0.5%
Slope of regression line (CDR)	-3.98E-3	-12E-3	-25.8E-3	-31.7E-3

Figure 3-21. List of wear index, weight loss part per thousand, and slope of regression line for by varying the volume percent of pigments adding- black paint/ 600C sand paper

Summary

Black superhydrophobic paint was made successfully by mixing fluorinated iron oxide particles and SBS. By adjusting V% of adding pigments, threshold value was found between 60V%~65V%, and samples with 65V%, 70V %, 75V% achieved superhydrophobicity after coating solidified. Two types of sand paper, which are 1200C and 600C, were used in Chapter 3 because CDR data shows that 1200C sand paper is too fine to destroy polymer matrix of black paint because the loss of weight for 4 samples are around 5~6%. Without destroying the polymer matrix, although decreasing the contact angle in 1200C abrasion test, four samples were in superhydrophobic regime after 400 cycles abrasion. Furthermore, 600C sand paper abrasion test expressed outcomes which are close to our expectation. Polymer matrix was destroyed layer by layer so that fluorinated particles which were buried in polymer matrix at beginning ascended to the top layer and formed random rough surface. This is the reason why water contact angle was trivial in the test abraded by 600C sand paper. For proving this explanation, CDR data under 600C sand paper abrasion is much higher than 1200C. 75V% sample lost 31% weight after 1000 times 600C sand paper abrasion which is 6 times higher than the results under 1200C. Superhydrophobic and durable black paint has been successfully fabricated with fluorinated iron oxide black matte and PVDF-PMMA mixed polymer with 65V%~75V% black pigments adding.

Superhydrophobic Blue Paint Fabrication and Characterization

Materials and Experimental Process

Fabrication of superhydrophobic blue pigments

Ultra-marine blue matte was purchased from Powdered-Up Dolly. The processing starts with, blue matte particles being dehydrated in the oven at 120C° and then dispersed in chloroform. Subsequently, heptadecafluoro-1, 1, 2, 2,-tetrahydrodecyltrichlorosilcane, which is from Gelest Inc., was added to the ultramarine-chloroform dispersion with the ratio 1ml : 1g blue matte and treated for 1h. Afterwards, centrifuging the dispersion and decanting the chloroform follows. Drying of particles is done at 120C° on a heating plate for 5hs. The fluorinated blue matte is obtained in this way.

Binder blending

Standard binder solution (SBS) was used for blue paint fabrication and the recipe is listed in white paint section.

Preparation of pure blue coating samples with different V%

After binder blending, adding pigments which are Ultra-marine blue matte with different volume percent which are 75% (with 1.04g fluorinated ultramarine adding), 70% (with 0.8g fluorinated ultramarine adding), 65% (with 0.64g fluorinated ultramarine adding), and 60% (with 0.52g fluorinated ultramarine adding). Stirring vigorously for 6h and are coated on the 1”x 1.5” soda-lime glass slide with 100 rpm rotation speed by spin coater. Then dry in air for 24 hrs.

Preparation of white-blue mixed paint

Blue#1 (B1) paint contains pure hydrophobized ultramarine 75V% as a superhydrophobicity contributor blended with the standard binder solution but paints B2 to B4 are fluorinated ultramarine adulteration in 65V% silica white paint. For example, B2 is 65 V% silica white paint blended with 0.1g ultramarine, B3 is with 0.2g ultramarine, and B4 is with 0.3g

ultramarine respectively. Because of different amount of adulteration, we are able to develop various blue paints.

Results and Discussion

Initial Contact Angel Measurement

In blue paint system, threshold value was found between 60V%~65V% (shown in Figure 3-22) and this number is almost identical to the value in black paint system. Random stacking empirical outcome can be used to explain why threshold value was detected in this range. Density of random close packing was found in the range of 56% -64% [33]. Above this value, polymer matrix distribution starts to change (shown in Figure 3-4) from funicular to pendular. With this shift, roughness of coating increases such that the contact angle also increases.

Recipe	Initial Water Contact Angle
1.04g pigments in SBS (Volume % of pigment: 75%)	153±2° 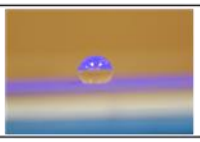
0.8 g pigments in SBS (Volume % of pigment: 70%)	151±2° 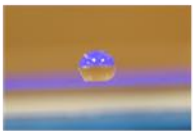
0.64g pigments in SBS (Volume % of pigment: 65%)	150±2° 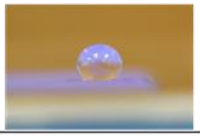
0.52g pigments in SBS (Volume % of pigment: 60%)	148±2° 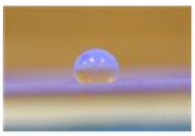

Figure 3-22. Initial contact angle of blue paint with different V%

Wear Resistance Test by Using 600C Sand Paper –Blue Paint

In abrasion test, 600C sand paper was selected to be the abrader in order to remove both particles and polymer matrix on the top layer. Interestingly, contact angle of blue paint decreases gradually while testing. From the data in Figure 3-23, contact angle of 4 samples with different

V% drops to 110°. We speculate the reason is that the structure of blue paint is stronger than black paint or white paint so that 600C sand paper was not able to destroy the polymer matrix. As a means to observe steady contact angle under abrasion test, polymer matrix should be erased layer by layer. Rougher sand paper is needed.

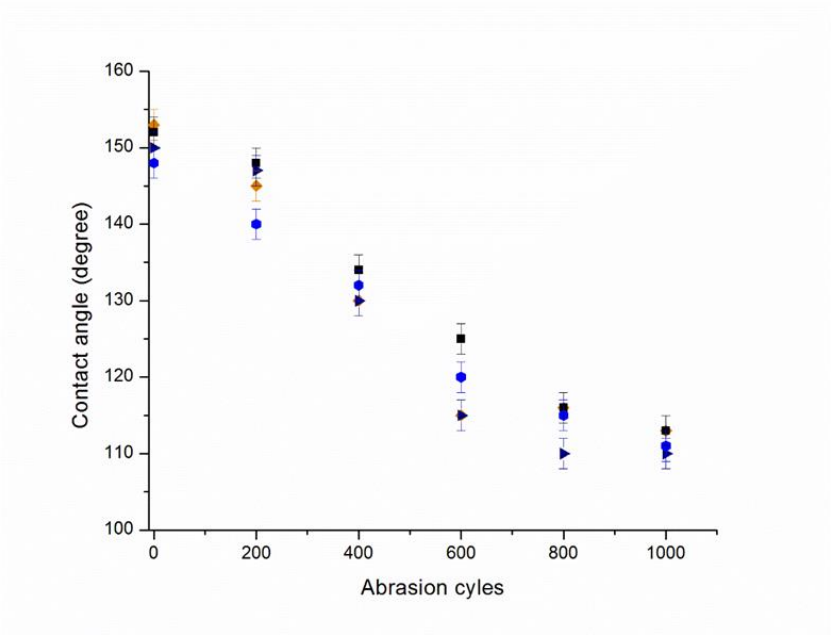

Figure 3-23. Contact angle decreases with abrasion cycles increase- blue paint/ 600C sand paper (♦: 75V%, ■: 70V%, ►:65 V%, ●: 60 V %)

Sample V%	●: 60 V%	►:65 V%	■: 70 V%	♦: 75 V%
Slope of regression line of contact angle change	-0.039	-0.046	-0.042	-0.043

Figure 3-24. Contact angle decreasing trend of -blue paint/ 600C sand paper

Figure 3-25 shows the CDR and wear index of samples with 75V%, 70V%, 65V% and 60V% pigments adding. Under abrasion of 600C sand paper, weight loss and CDR of four samples are quite similar which are all around 5~6 % and this number is close to the loss of black sample under 1200C abrasion test. This consequence demonstrated the explanation in the

previous section. Wear resistance of blue paint is stronger so that even 600C sand paper was only able to remove particles such that the retained polymer was compressed by abrader loading and contact angle decline was observed

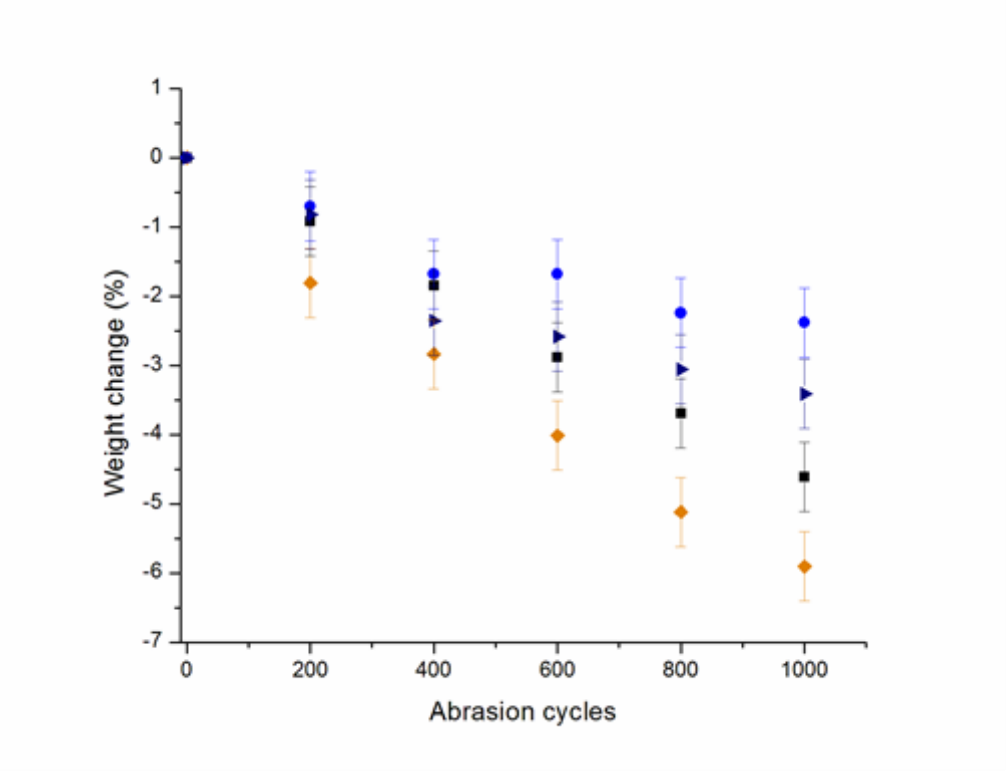

Figure 3-25. Weight change against abrasion cycles increase-blue paint/ 600C sand paper (♦: 75V%, ■: 70V%, ►:65 V%, ●: 60 V %)

Sample V%	●: 60 V%	►:65 V%	■: 70 V%	♦: 75 V%
Wear Index (mg/cycle)	-7.5 E-3	-1.7E-3	-4E-3	-7.5E-3
Percentage of weight change to initial weight after 1000 cycles abrasion (%)	-3.4±0.5%	-2.38±0.5%	-4.6±0.5%	-5.9±0.5%
Slope of regression line (CDR)	-3.4E-3	-2.3E-3	-4.6E-3	-5.8E-3

Figure 3-26. List of wear index, weight loss (%), and slope of regression line for by varying the volume percent of pigments adding - blue paint/ 600C sand paper

White Paint Blended by Blue Pigments

B1 is the pure blue paint with 75V% fluorinated ultramarine adding. B2~B4 are 65V% white paint with 0.1g, 0.2g, 0.3g fluorinated ultramarine adding, respectively. Figure 3-27 shows the appearance of samples and initial contact angle measurements were also reported in Figure 3-27. B1-B4 expressed superhydrophobicity after coating was dried in air for 24hrs. With this effect, we know fluorinated color pigments can be blended together for color adjusting. Contact angle changing against abrasion cycles for B1-B4 was show in Figure 3-28. Trend of B1is similar comparing to the previous result. In samples B2-B4, with more blue matte adding, structure was getting weaker so that 600C sand paper can deplete the polymer matrix. Hence, contact angle were still above 150° after 1000 time abrasion.

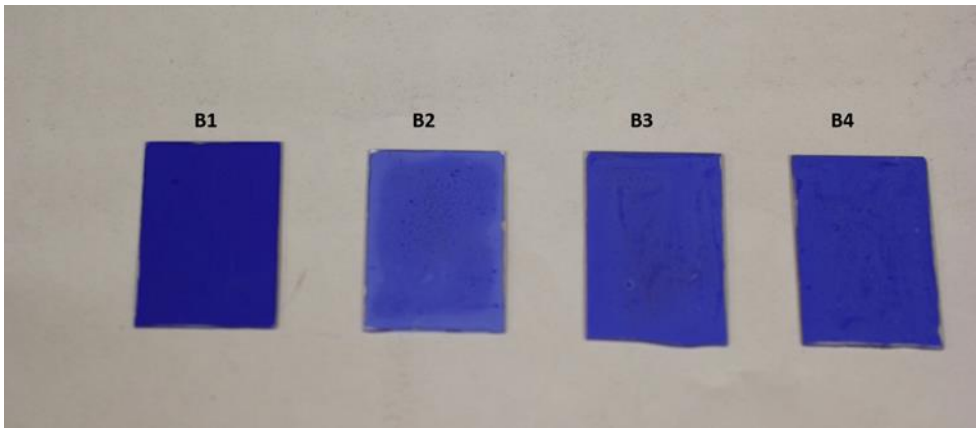

Figure 3-27. Appearances of B1 to B4. (Photo courtesy of author)

75 V% blue paint - B1	Ultramarine 0.1g in 65V% white paint -B2	Ultramarine 0.2g in 65V% white paint –B3	Ultramarine 0.3g in 65V% white paint –B4
WCA: 150°±3°	WCA: 153°±3°	WCA: 151°±3°	WCA: 149°±3°
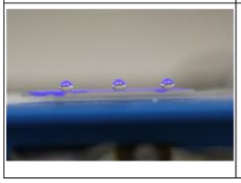	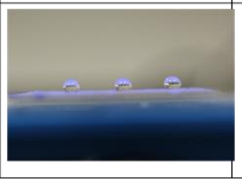	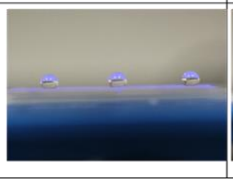	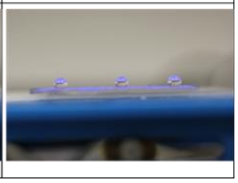

Figure 3-28. DI water contact angle for B1~B4 samples. (Photo courtesy of author)

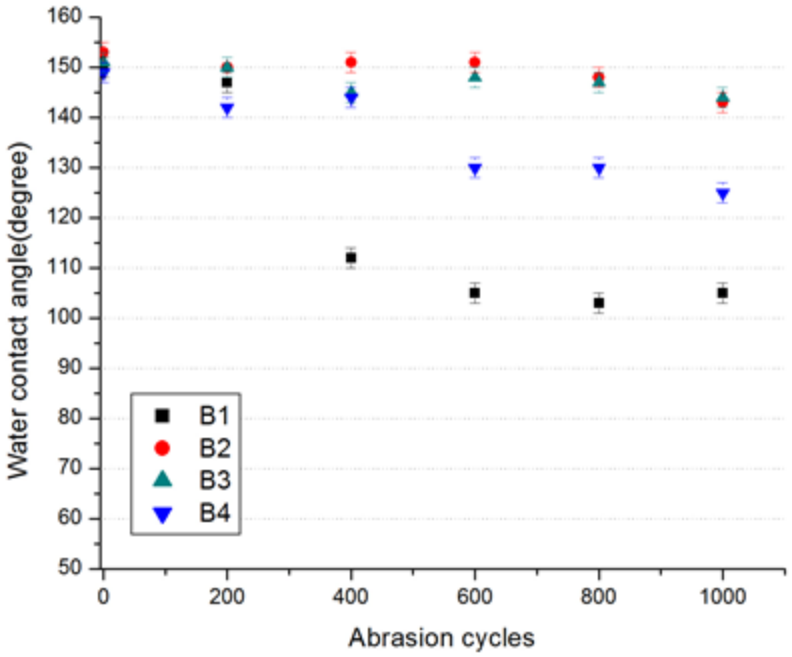

Figure 3-29. Change of contact angle with increasing of abrasion cycles for white-blue mixed paint system

Summary

Blue superhydrophobic paint was successfully fabricated by following the logic of new design. By varying the V% adding, threshold value to achieve superhydrophobicity was found between 60V%-65V% in blue paint system. However, water contact angle didn't show stability neither under 1200C sand paper nor 600C sand paper. This phenomenon is quite different from other 4 paints. The reason is that polymer matrix was not damaged by these two sand paper so that the lower level of particles is still implanted in polymer matrix. In doing so, roughness factor decreases while abrasion, so contact angle declined to intrinsic contact angle of PVDF-PMMA mixed polymer. With rougher sand paper like 300C or even 120C, blue paint may be able to remain in superhydrophobic regime after 1000 times abrasion.To conclude, superhydrophobic and durable blue paint has been successfully fabricated with fluorinated ultramarine blue matte

and PVDF-PMMA mixed polymer with 65V%~75V% .This data is also the first quantitative data to describe durability of superhydrophobic blue coating.

Superhydrophobic Green Paint Fabrication and Characterization

Materials and Experimental Process

Fabrication of superhydrophobic green pigments

Chromium oxide green matte was purchased from Powdered-Up Dolly. The processing starts with, chromium oxide green matte particles being dehydrated in the oven at 120C° and then dispersed in chloroform. Subsequently, heptadecafluoro-1, 1, 2, 2,-tetrahydrodecyltrichlorosilcane, which is from Gelest Inc., was added to the chromium oxide - chloroform dispersion with the ratio 1ml : 1g green matte and treated for 1h. Afterward, centrifuging the dispersion and decanting the chloroform follows. Drying of particles is done at 120C° on a heating plate for 5hs. The fluorinated green matte is obtained in this way.

Binder blending

Standard binder solution (SBS) was used for green paint fabrication and the recipe is listed in white paint section.

Preparation of pure green coating samples with different V%

After binder blending, adding pigments which are chromium oxide green matte with different volume percent which are 75% (with 2.27g fluorinated green matte adding), 70% (with 1.79 fluorinated green matte adding), 65% (with 1.46g fluorinated green matte adding), and 60% (with 1.12g fluorinated green matte adding). Stirring vigorously for 6h and are coated on the 1”x 1.5” soda-lime glass slide with 100 rpm rotation speed by spin coater. Then dry in air for 24 hrs.

Preparation of white-green mixed paint

Green #1 (G1) paint contains pure hydrophobized green matte 75V% as a superhydrophobicity contributor and then blended with the standard binder solution but paints

G2 to G4 are fluorinated green matte adulteration in 65V% silica white paint. For example, G2 is 65 V% silica white paint blending with 0.1g fluorinated green matte adding, G3 is with 0.2g fluorinated green matte adding, and G4 is with 0.3g fluorinated green matte adding, respectively. The logic of white-blue mixed paint was follower to develop various green paints.

Initial Contact Angle of Coating with Different V% Pigments

Recipe	Initial Water Contact Angle
2.27g pigments in SBS (Volume % of pigment: 75%)	155±2° 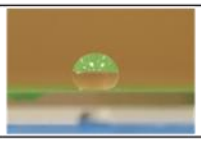
1.79g pigments in SBS (Volume % of pigment: 70%)	153±2° 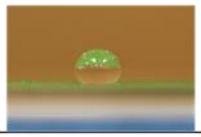
1.46g pigments in SBS (Volume % of pigment: 65%)	151±2° 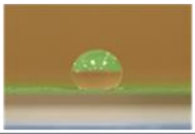
1.12g pigments in SBS (Volume % of pigment: 60%)	148±2° 

Figure 3-30. Higher pigment volume percent yields higher initial contact angle -green paint system

Wear Resistance Test by Using 600C Sand Paper –Green Paint

Figure 3-31 provides the contact angle changing against abrasion cycles for green paint. As the data shown, contact angle of coating fluctuated because the polymer matrix was destroyed and this phenomenon matched our expectation. 75V% green paint possessed 154° contact angle after 1000 times abrasion and other 3 samples were also in superhydrophobic regime.

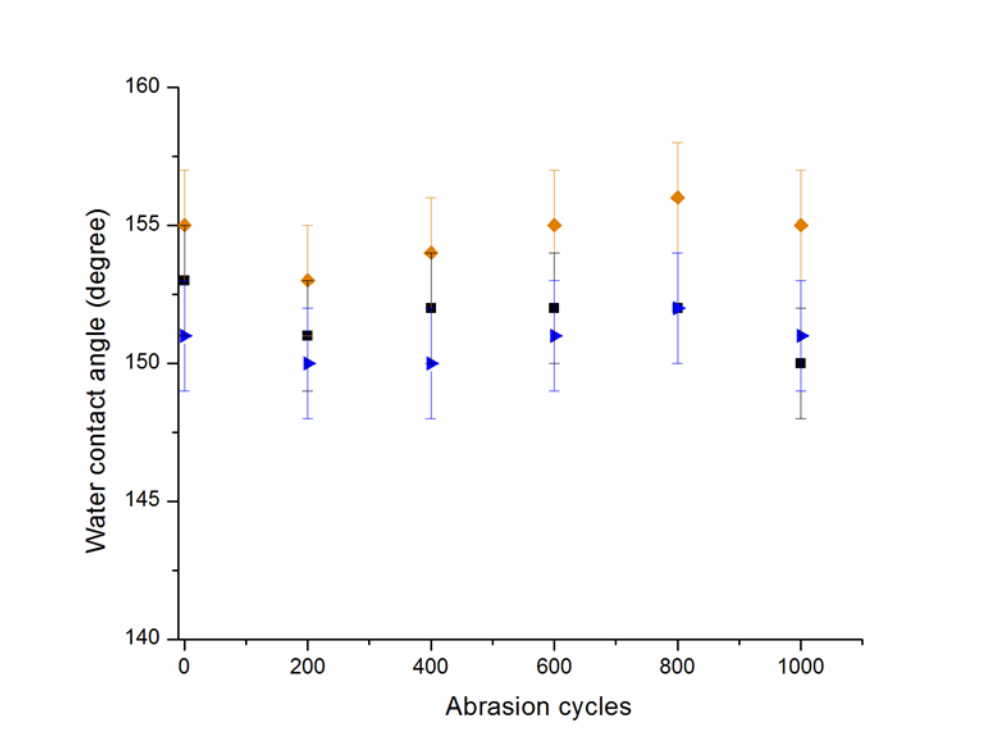

Figure 3-31. Contact angle fluctuates with abrasion cycles increase- green paint/ 600C sand paper (♦: 75V%, ■: 70V%, ►:65 V %)

Sample V%	►:65 V%	■: 70 V%	♦: 75 V%
Slope of regression line of contact angle change	1E-3	-0.002	0.0014

Figure 3-32. Contact angle changing trend of -green paint/ 600C sand paper

Figure 3-33 gives the weight change of samples, which are 75%, 70%, 65%, and CDR was calculated by regression line program with 99% confidence. The calculated values are shown in the Figure 3-34, 75V% one lost 9.26% of weight which is the highest among these samples because higher V% pigments adding gave fragile structure but yielded better wettability. From the facts of weight loss, we know the polymer matrix was destroyed so the wettability was steady due to new layer of particles ascended to the top.

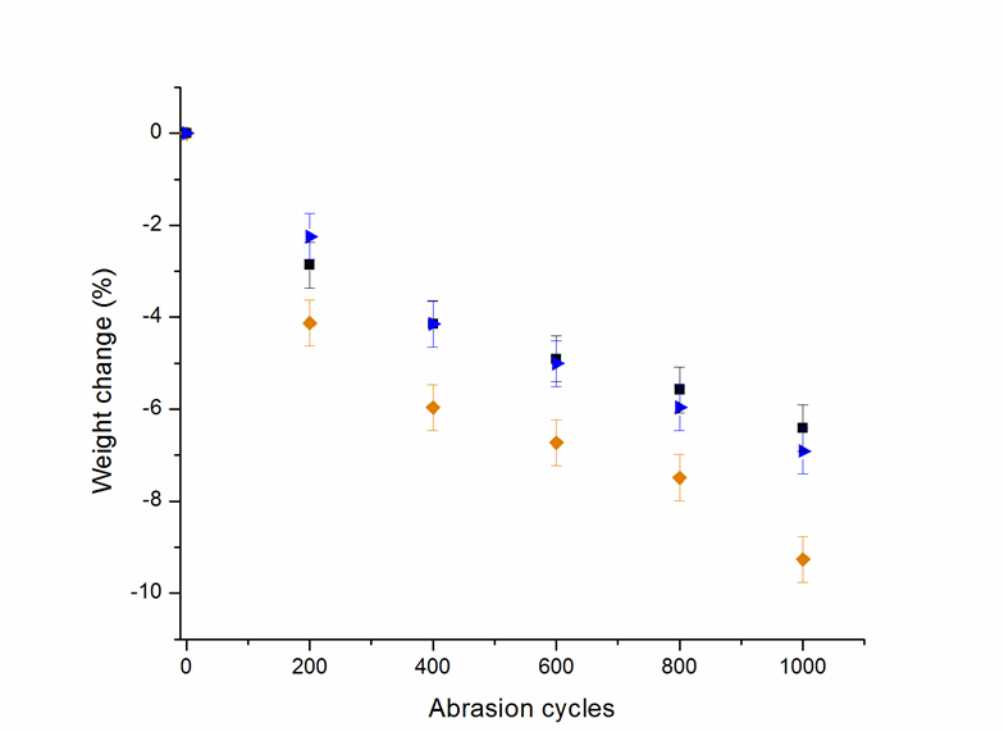

Figure 3-33. Weight change in percentage against abrasion cycles increase– green paint/ 600C sand paper (♦: 75V%, ■: 70V%, ►:65 V %)

Sample V%	►:65 V%	■: 70 V%	♦: 75 V%
Wear Index (mg/cycle)	-8E-3	-8.5E-3	-0.014
Percentage of weight change to initial weight after 1000 cycles abrasion (%)	-6.9±0.5%	-6.4±0.5%	-9.26±0.5%
Slope of regression line (CDR)	-6.7E-3	-5.9E-3	-8E-3

Figure 3-34. List of wear index, weight loss (%), and slope of regression line (CDR) for by varying the volume percent of pigments adding - green paint/ 600C sand paper

White Paint Blended by Green Pigments

G1 is the green paint with 75V% fluorinated chromium oxide green matte adding. G2~G4 were 65V% white paint with 0.1g, 0.2g, 0.3g fluorinated chromium oxide green matte adulterated, respectively. Figure 3-35 shows the appearance of samples. Initial contact angle measurements were also reported in Figure 3-36. Depending on the results, G1~G4 expressed

superhydrophobicity after coating was dried in air for 24hrs. Contact angle changing against abrasion cycles for G1-G4 was show in Figure 3-36. All 4 samples possess superhydrophobicity after 1000 times abrasion by 600C sand paper.

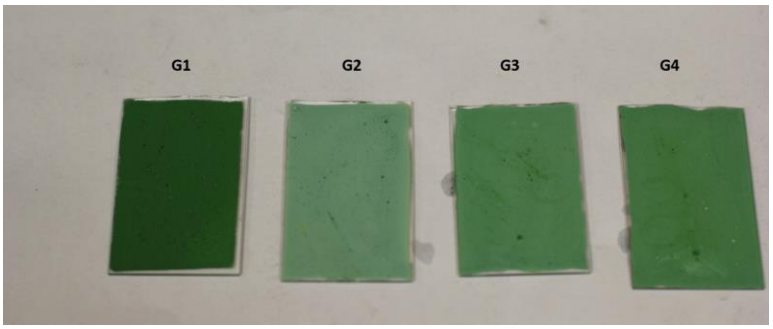

Figure 3-35. Appearances of G1 to G4, G1 is 75V% pure green paint, G2~G3 are green pigments adulterated white paint. (Photo courtesy of author)

75 V% green paint - G1	Chromium oxide green matte 0.1g in 65V% white paint - G2	Chromium oxide green matte 0.2g in 65V% white paint – G3	Chromium oxide green matte 0.3g in 65V% white paint – G4
WCA: 160°±3°	WCA: 155°±3°	WCA: 160°±3°	WCA: 161°±3°
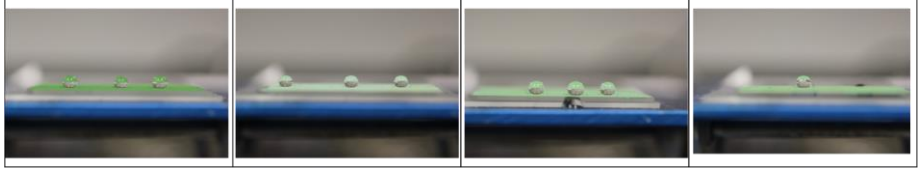			

Figure 3-36. Initial contact angle of G1~G4. (Photo courtesy of author)

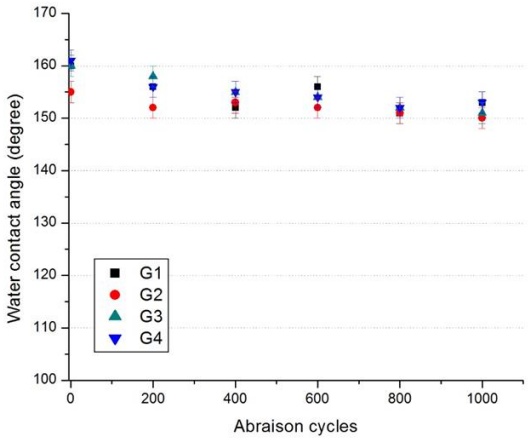

Figure 3-37. Change of contact angle with increasing of abrasion cycles for white-green mixed paint

Summary

Green superhydrophobic paint was successfully made by following the logic of new design, which is the volumetric superhydrophobic coating. Because there is a trade-off between wettability of coating and wear resistance, threshold value to achieve superhydrophobicity should be demonstrated. By varying the V% adding, threshold value to achieve superhydrophobicity was found between 60V% ~65V% in green paint system. Experiment for Contact angle change against abrasion cycles was done by Taber linear abraser with 600C sand paper as an abrader. This data shows that three samples, which are 65V%, 70V% and 75V%, are still in superhydrophobic regime after 1000 times abrasion. Weight loss of coatings were also measured and the CDR of these 3 samples was also calculated. 75V% loss 9.26% after 1000 times abrasion which means 75V% coating may survive up to 10000 times abrasion. Moreover, 70V% and 65V% lost only 5% after 1000 times abrasion which are more rigid than 75%. Fluorinated green matte also could be used to adulterate our white paint system in order to adjust color to satisfy demanding circumstances.

To conclude, superhydrophobic and durable green paint has been successfully fabricated with fluorinated chromium oxide green matte and PVDF-PMMA mixed polymer with 65V%~75V% green pigments adding. This data is also the first quantitative data to describe durability of superhydrophobic coating.

Superhydrophobic Red Paint Fabrication and Characterization

Materials and Methods

Fabrication of superhydrophobic red pigments

Iron oxide red matte was purchased from Powdered-Up Dolly. The processing starts with, Iron oxide red matte particles being dehydrated in the oven at 120C° and then dispersed in chloroform. Subsequently, heptadecafluoro-1, 1, 2, 2,-tetrahydrodecyltrichlorosilcane, which is

from Gelest Inc., was added to the iron oxide -chloroform dispersion with the ratio 1ml: 1g red matte and treated for 1h. Afterward, centrifuging the dispersion and decanting the chloroform follows. Drying of particles is done at 120C° on a heating plate for 5hs. The fluorinated red matte is obtained in this way.

Binder blending

Standard binder solution (SBS) was used for red paint fabrication and the recipe is listed in white paint section.

Preparation of pure red coating samples with different V%

Adding fluorinated iron oxide red matte with different volume percent which are 75% (with 2.26g fluorinated iron oxide adding), 70% (with 1.78 fluorinated iron oxide adding), 65% (with 1.45g fluorinated iron oxide adding), and 60% (with 1.11g fluorinated iron oxide adding). Stirring vigorously for 6h and are coated on the 1”x 1.5” soda-lime glass slide with 100 rpm rotation speed by spin coater. Then dry in air for 24 hrs.

Preparation of white-red mixed paint

Red #1 (R1) paint contains 75V%pure hydrophobized red mattes as a superhydrophobicity contributor and then blended with the standard binder solution but paints R2 to R4 are fluorinated red matte adulteration in 65V% silica white paint. For example, R2 is 65 V% silica white paint blending with 0.1g fluorinated red matte adding, R3 is with 0.2g fluorinated red matte adding, and R4 is with 0.3g fluorinated red matte adding, respectively.

Results and Discussion

Initial Contact Angle Measurements- Red Paint

In red paint system, threshold value was also found between 65V%~70V% and this value is close to the range of possible density of random close packing which is 56% -64% and complied with our expectation. Polymer distribution shifts from saturated to pendular with

decreasing volume percent of polymer. Figure 3-38 gives the results that higher V% paint yields higher initial contact angle and this also fulfills our prediction due to the higher roughness factor in high V% system.

Recipe	Initial Water Contact Angle
2.26g pigments in SBS (Volume % of pigment: 75%)	154±2° 
1.78g pigments in SBS (Volume % of pigment: 70%)	151±2° 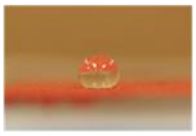
1.45g pigments in SBS (Volume % of pigment: 65%)	145±2° 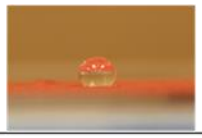
1.11g pigments in SBS (Volume % of pigment: 60%)	143±2° 

Figure 3-38. Higher pigment volume percent yields higher initial contact angle -red paint system

Abrasion Test by Using 600c Sand Paper – Red Paint

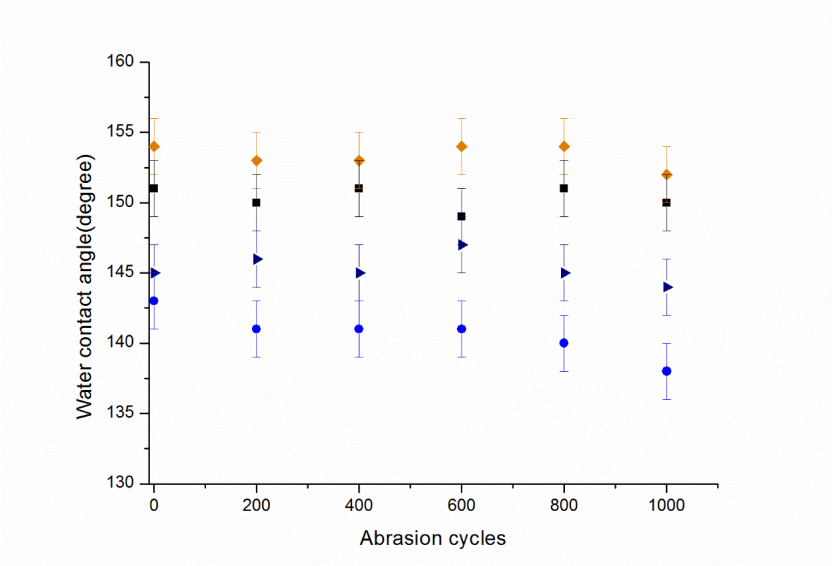

Figure 3-39. Contact angle fluctuates with abrasion cycles increase- red paint/ 600C sand paper (♦: 75V%, ■: 70V%, ►:65 V%, ●: 60 V%)

Contact angle change against abrasion cycles increase was listed in the Figure 3-39 and we can see them fluctuate and the values were close to the initial contact angle of each of them after abrasion. Explanation for other color paint systems is also fitting here. 600C sand paper was rough enough to destroyed polymer matrix so that new rough surface came out and hold superhydrophobicity after abrasion.

Sample V%	●: 60 V%	►:65 V%	■: 70 V%	♦: 75 V%
Slope of regression line of contact angle change	-0.004	-8.6E-4-	-5.7E-4	-8.6E-4

Figure 3-40. Contact angle changing trend of -red paint/ 600C sand paper

In red superhydrophobic paint system, 75V% paint lost 31% of weight after 1000 abrasion but CDR of red paint was twice of the other three samples. We speculate that polymer distribution shifted from funicular to pendular so that 75V% is much more fragile than others.

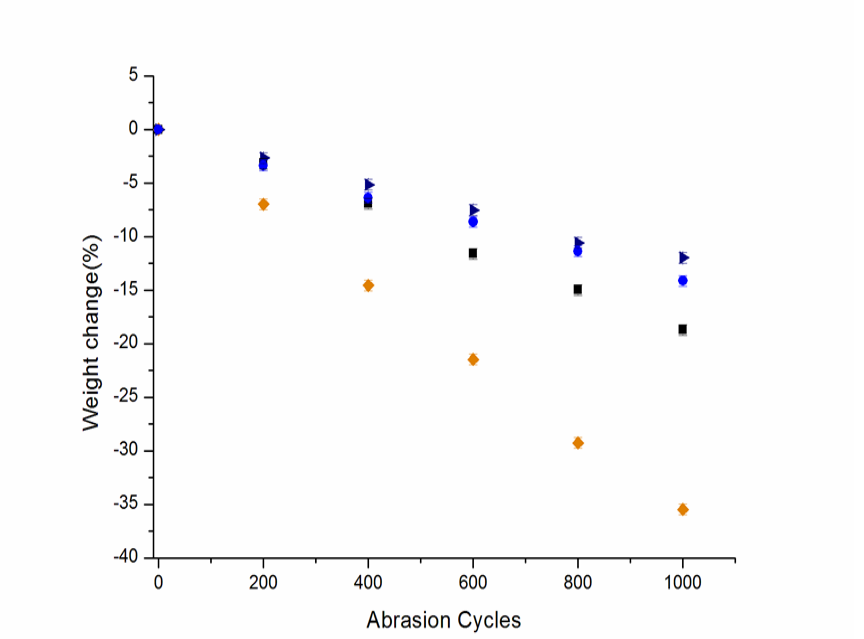

Figure 3-41. Weight change in percentage against abrasion cycles increase– red paint/ 600C sand paper (♦: 75V%, ■: 70V%, ►:65 V %, ●: 60 V %)

Sample V%	●: 60 V%	►:65 V%	■: 70 V%	♦: 75 V%
Wear Index (mg/cycle)	-0.01	-8.6E-3	-0.02	-0.07
Percentage of weight change to initial weight after 1000 cycles abrasion (%)	-14±0.5%	-12±0.5%	-18.7±0.5%	-35.5±0.5%
Slope of regression line (CDR)	-0.013	-0.012	-0.019	-0.036

Figure 3-42. List of wear index, weight loss (%), and slope of regression line (CDR) for by varying the volume percent of pigments adding - red paint/ 600C sand paper

White Paint Blended by Red Pigments

R1 is the red paint with 75V% fluorinated iron oxide red matte adding. R2~R4 were 65V% white paint with 0.1g, 0.2g, 0.3g fluorinated iron oxide red matte adulterated, respectively. Figure 3-34 shows the appearance of samples. Initial contact angle measurements were also reported in Figure 3-44. Depending on the results, R1~R4 possessed superhydrophobicity after coating was dried in air for 24hrs. Contact angle changing against abrasion cycles for R1-R4 was show in Figure-34. All 4 samples were in superhydrophobic regime after 1000 times abrasion by 600C sand paper.

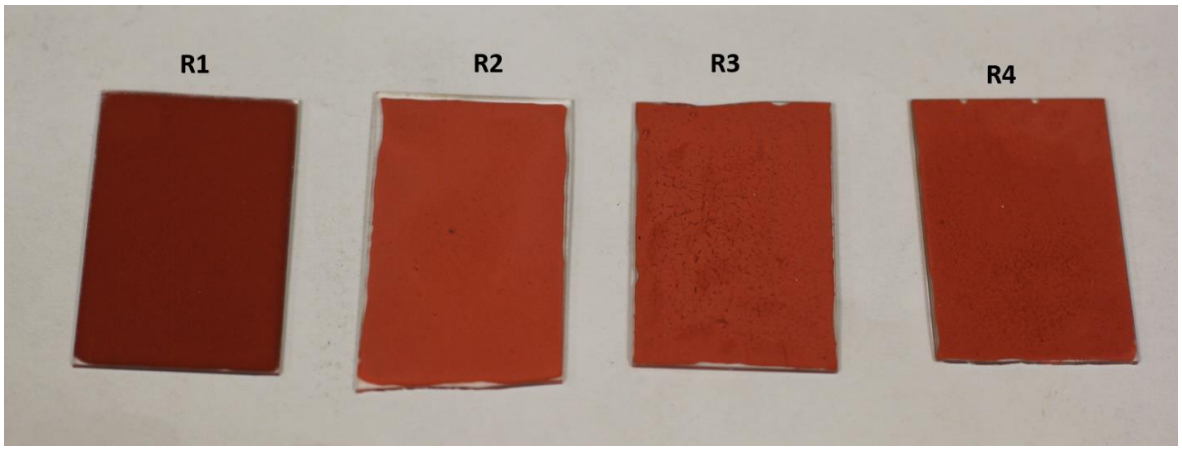

Figure 3-43. Appearances of R1 to R4, R1 is 75V% pure red paint, R2~R3 are red pigments adulterated white paint. (Photo courtesy of author)

75 V% red paint - R1	Iron oxide red matte 0.1g in 65V% white paint -R2	Iron oxide red matte 0.2g in 65V% white paint –R3	Iron oxide red matte 0.3g in 65V% white paint –R4
WCA: 159°±3°	WCA: 153°±3°	WCA: 153°±3°	WCA: 150°±3°
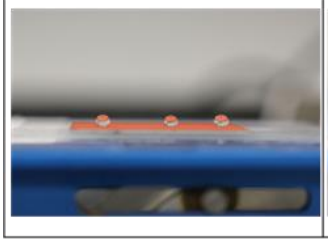	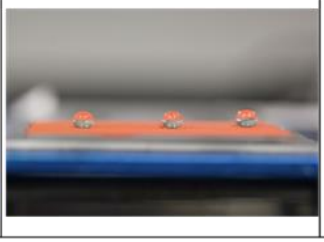	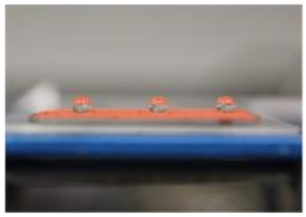	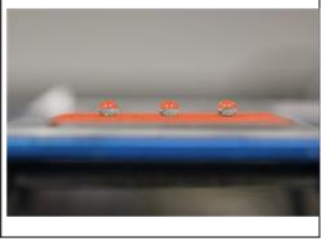

Figure 3-44. Initial contact angle of R1-R4. (Photo courtesy of author)

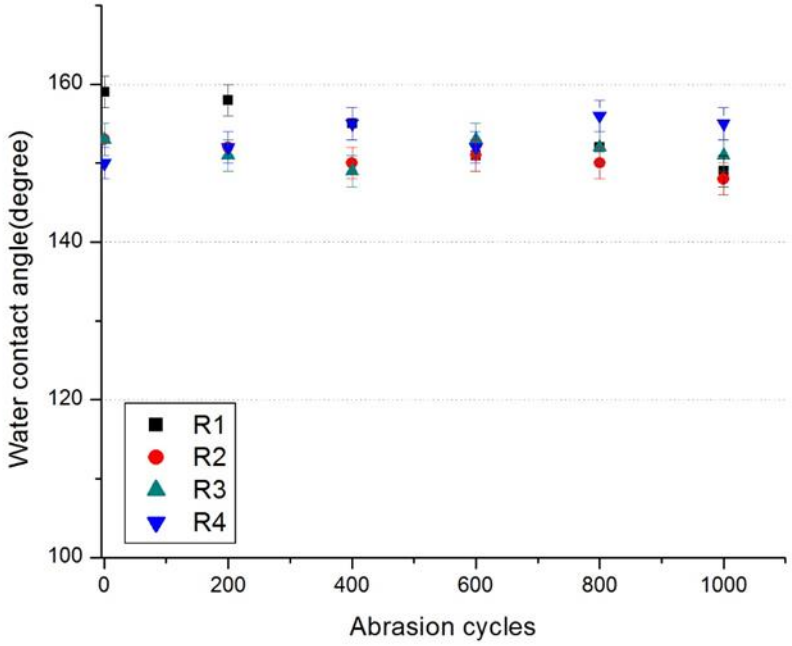

Figure 3-45. Change of contact angle with increasing of abrasion cycles for white-red mixed paint

Summary

Red superhydrophobic paint was successfully fabricated by following the logic of new design. Because there is a trade-off between wettability of coating and wear resistance, threshold value to achieve superhydrophobicity should be demonstrated. By varying the V% adding,

threshold value to achieve red superhydrophobicity was found between 65V%-70V% in red paint system. Experiment for contact angle change against abrasion cycles was done by Taber linear abraser with 600C sand paper as an abrader. 70V% and 75V% samples are still in superhydrophobic regime after 1000 times abrasion. Weight loss of coatings were also measured and the CDR of samples was also calculated. Because black and red paint are iron oxide based paint so the adhesion between particle and polymer is almost identical. Weight change after abrasion was similar to the data of black paint. To conclude, superhydrophobic and durable red paint has been successfully fabricated with fluorinated iron oxide red matte and PVDF-PMMA mixed polymer with 65V%~75V% red pigments adding. This data is also the first quantitative data to describe durability of superhydrophobic red coating.

Discussion and Understanding

In Figure 3-46, transitions point to achieve superhydrophobicity were discovered between 60V% to 70V% for four sorts of paints. Interestingly, pigments used for 4 sorts of paint were different which are iron (II) oxide (black), iron (III) oxide (red), chromium (III) oxide and Ultramarine (blue). Figure 3-47 shows the structure of particle-polymer composite with different ratio of particle. Structure shifts to funicular structure from capillary structure once particle volume percent is higher than 65% and contribute to higher wall roughness. 65V% is also the upper limit of random close packing density. Therefore, this dissertation demonstrated a general principle for volumetric superhydrophobic coating fabrication. By adjusting the volume percent of particles, coating can attain superhydrophobic as long as particle volume percent is higher than 65V%. However, coating with higher particle volume percent yields a weaker structure. Therefore, 60V% ~ 70V% is the most appropriate to balance wettability and durability.

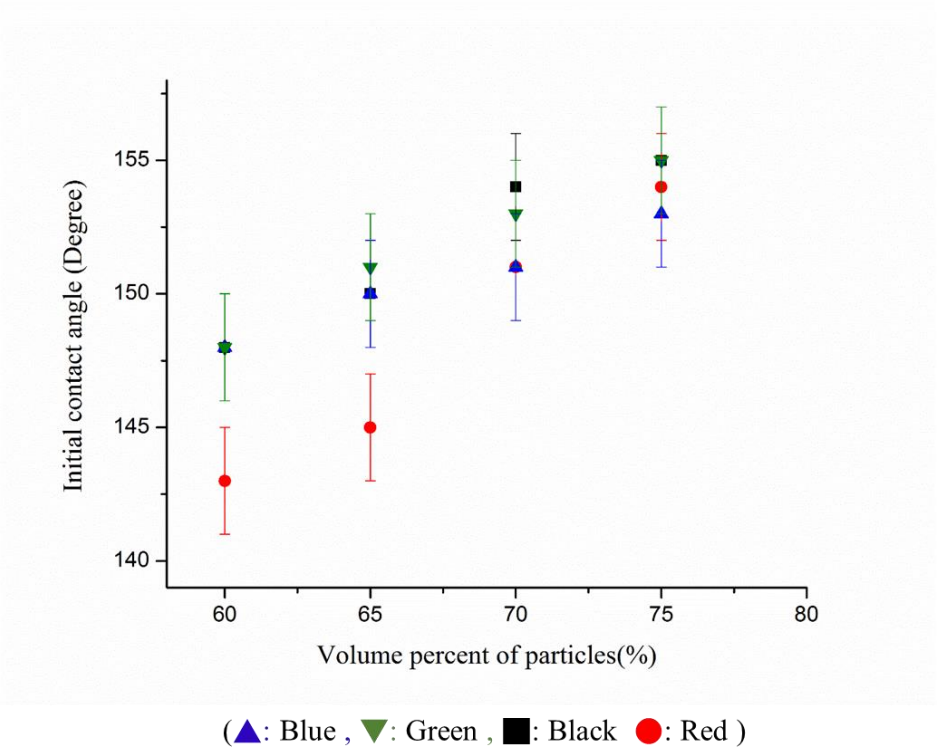

Figure 3-46. Correlation of initial contact angle and volume percent of particles

Volume percent of particles				
0-10%	10-65%	65-90%	90-100%	100%
Saturated	Capillary	Funicular	Pendular	Dry
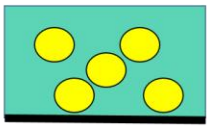	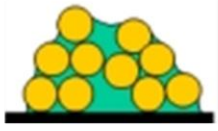	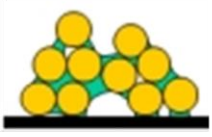	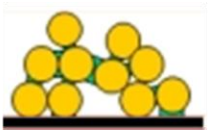	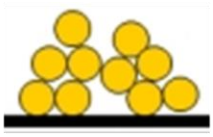

Figure 3-47. Different ratio of particle and polymer turns out different structure

Chapter Conclusion

In Chapter 3, five sorts of durable superhydrophobic paints were invented by blending selected fluorinated color matte and standard binder solution. By adjusting the volume percent of

added pigment, threshold to achieve superhydrophobic was found for 5 sorts of paint. The thresholds are in the range of 60V%~70V% which is the possible maximum packing density of random packaging. Once particle volume ratio is above this range, structure of coating turned from thin-film like structure to fluffy. With fluffy structure, roughness factor strongly increases. However, strength of structure descends dramatically so CDR is around 200% than the thin-film like structure. Nevertheless, polymer is distributed between particles and this is why fluffy structure retains decent durability. On the other hand, this work also demonstrates the ability to use modified ASTM standards to characterize the durability of superhydrophobic surfaces. The data that needs to be collected is the water contact angle change vs. the number of abrasion cycles, the weight loss vs the number of abrasion cycles. The hope is that this approach can be the basis for a new ASTM standard.

CHAPTER 4
FABRICATION OF DURABLE SUPERHYDROPHOBIC AND TRANSPARENT COATING VIA SILICA SOL-GEL COVER LAYER

Introduction

The purpose of Chapter 4 is to investigate a new method to strengthen the surface feature of a transparent and superhydrophobic coating by using monodisperse nanoparticles and silica sol-gel cover layer. The material chosen in Chapter 4 is silicon dioxide (SiO2) which is synthesized from tetraethyl orthosilicate (TEOS) by the Stöber process. Silica sol was also synthesized from TEOS with an acidic catalyst and played a role of binder in Chapter 4.

To achieve superhydrophobicity, heptadecafluoro-1 1 2 2-tetrahydrodecyl trichlorosilane was applied on the surface of silica cover layer and silica particles for improvement of surface chemistry. Contact angle change against abrasion cycles and transmittance are reported in Chapter 4

Background

To achieve transparent and superhydrophobic surface, light scattering theory was referred to explain how to build surface features but reduce light scattering.

Light Scattering Theory

Formal light scattering theory can be categorized in two frameworks. One is the theory of Rayleigh scattering (after Lord Rayleigh)[58], [59] and another is Mie scattering (after Gustav Mie)[60]–[62]. Rayleigh is applicable to small, dielectric (non-absorbing), spherical particles. Mie scattering has no size limitations and can be used to describe most spherical particle scattering systems. Rayleigh scattering and Mie scattering are used in different criteria described by the dimensionless size parameter (α):

$$\alpha = \frac{2\pi a}{\lambda} \tag{4-1}$$

Where α is the spherical particle radius, and λ is the relative scattering wavelength.

Depending on α, there are three regimes that correspond to scattering theory.

- α <<1: Rayleigh scattering (small particle compared to wavelength of light)
- α ≈1 : Mie scattering (particle is about the same size as wavelength of light, valid only for spheres)
- α >>1: Geometric scattering (particle much larger than wavelength of light)

In Chapter 4, we are going to develop a coating that is transparent in the visible light range (400-700nm) and the size of nanoparticle is 50nm to 60nm. Therefore, Mie scattering is a more reasonable model to illustrate the scattering behavior in this proposal.

For optimizing the superhydrophobic property, raising the surface roughness is required. However, increasing of the feature size of the surface causes scattering to be more and more conspicuous. As mentioned above, the Mie scattering theory is commonly used to describe the interaction between the surface roughness and incident visible light. According to Mie theory, the scattering cross-section (C_{sca}) is given by:

$$C_{sca} \approx \frac{\pi d^2}{2} \sum_{n=1}^{\infty} (2n+1)(a_n + b_n) \qquad (4\text{-}2)$$

Where, the d is the particle diameter and the a_n and b_n are Mie coefficient of the order n, which are related to the material property. C_{sca} is proportional to d^2, however, surface features are necessary for superhydrophobicity. It expresses there is upper limit of transparency with which the coating can still perform superhydrophobicity.

Silica Nanoparticles Synthesis via Stöber Process

Stöber process is a common process for the generation of monodisperse nano silica particles. This process was published in 1968 by Werner Stöber et al [63]. Briefly speaking, silicon alkoxides like tetramethoxysilane (TMOS), tetramethoxysilane (TEOS), etc. as the

precursor were added to a low-molar mass alcohol such as ethanol or methanol and small amounts of ammonia were used as a catalyst. The general steps are:

1. Hydrolysis

   The hydrolysis reaction is:

$$\equiv Si - OR + H_2O \leftrightarrows \equiv Si - OH + ROH \tag{4-3}$$

2. Polymerization

$$\equiv Si - OH + OH^- \underset{fast}{\longrightarrow} \equiv Si - O^- + H_2O \tag{4-4}$$

$$\equiv Si - O^- + HO - Si \underset{slow}{\longrightarrow} \equiv Si - O - Si \equiv \ + OH^- \tag{4-5}$$

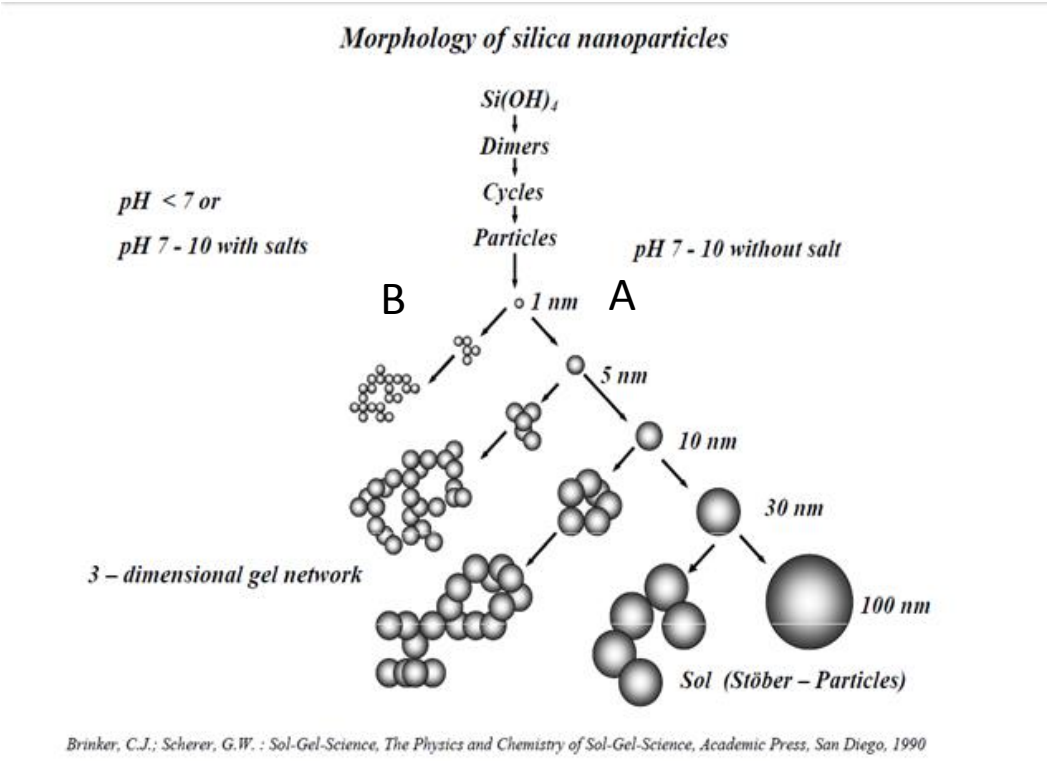

Figure 4-1.Polymerization behavior of aqueous silica. In basic condition. A) particles grow in size with decrease in number; however, B)in acidic condition or in presence of flocculation salts, particles tend to agglomerate into three dimensional networks and form gels. From Iler[64]

Silicic acid solutions slowly become thicker and finally gel, and most researchers prior to 1979 believed that Si(OH)4 polymerized into siloxane and cross linked like other organic polymers[64]. However, Iler reported that there is no relation or analogy between silicic acid polymerized in an aqueous system and condensation-type organic polymers. Instead, silicic acid polymerizes into discrete particles that in turn aggregate into chains and networks as first recognized by Carmen. According to Iler[64], polymerization occurs in 3 stages:

1. Polymerization of monomer to form particles
2. Growth of the particles.
3. Linking of particles into chains, then networks that extend throughout the liquid medium, thickening it to a gel.

pH –Dependence

In terms of silica polymerization behavior, pH value plays a significant role, and is discussed in detail in the following statements.

There are three pH domains of polymerization process reported by Iler which are < pH 2, pH 2-7 and > pH7. The reasons why Iler selected pH2 and pH7 as boundaries is that the point of zero charge (PZC) and isoelectric point (IEP) are in the range of pH1~pH3. PZC means the surface charge is zero and IEP means electrical mobility of the silica particles is zero. pH 7 is a boundary because the silica particles are noticeably ionized above pH7 and the particles grow without aggregation and gelation. The main mechanism of the Stöber process is in the range of pH7 to pH10.

Polymerization above ph7

Above pH 7, which is the route B in the Figure 4-1, polymerization takes place in two nucleophilic reactions:

$$\equiv Si - OH + OH^- \underset{fast}{\longrightarrow} \equiv Si - O^- + H_2O \quad (4\text{-}6)$$

$$\equiv Si - O^- + HO - Si \underset{slow}{\longrightarrow} \equiv Si - O - Si \equiv \ + OH^- \quad (4\text{-}7)$$

Nevertheless, condensed species will probably be ionized and therefore become repulsive to each other. Hence, growth is mainly caused by the addition of monomers to more highly condensed particles rather than by particle aggregation. Moreover, due to the greater solubility of silica and the greater size- dependence of solubility above pH7, growth of the primary particles continues by Ostwald ripening. Particles grow rapidly to a size that depends mainly on the temperature. (Particles grow in larger size with higher temperature because of the higher solubility of silica). Since growth occurs by the dissolution of smaller particles and deposition of soluble silica on larger particles, the growth rate depends on the particle-size distribution [65], [66].

Fundamental of Sol-Gel Dip Coating

Sol-gel dip coating is a conventional thin film deposition process. Compare to other thin-film deposition technique such as sputtering, evaporation, or chemical vapor deposition (CVD), dip coating relatively needs less equipment and is less costly. Scriven [38] divided dip coating process to 5 steps which are immersion, start-up, deposition &drainage, drainage, solvent evaporation. Final film thickness is determined by six forces[67], [68] which are 1) viscous drag upward on the liquid by the moving substrate , 2) force of gravity, 3) resultant force of surface tension in the concavely curved meniscus 4) inertial force of the boundary layer liquid ,5) surface tension gradient, and 6) the disjoining or conjoining pressure. From the report written by Strawbridge and James[69], they determined the relationship between silicate solution viscosity and thickness. The trend was found that higher viscosity results in thicker film in a fixed withdrawal speed. Here is why we set silicate sol V% as a parameter and try to find threshold

value of film thickness which possess relative strength but not fully bury the silica nanoparticles layer.

Materials and Methods

Silica nanoparticles synthesis (stöber process)

Stöber process was used to synthesize silica nanoparticles with 40nm diameter. 8.33g of tetra ethyl silicate (TEOS), 5g of de-ionized water, and 0.98g of 0.28N aqueous ammonium hydroxide solution were added to 100ml 99% ethanol and agitated for 24hours at 50°C. This process generated monodisperse silica nanoparticles of ~40 nm, as measured by SEM.

Silica sol-gel synthesis

With acidic condition catalyzed, silica precursor formed a thin film structure, which differed from forming monodisperse nanoparticles in basic condition. The reactants are de-ionized water 28.8g, ethanol 18.4g (assay: 99%), TEOS 20.8g (assay: 99%), 1ml 1M Hydrogen chloride solution. The total molar ratio is TEOS: water: Ethanol is 1:16:4. After sol-gel solution is prepared, the silica sol-gel and ethanol was mixed with different volume percents which are 1%, 2%, 3%, 4%, and 5%.

Silica nanoparticles deposition

The solvent for dispersing nanoparticles was ethanol. Best results were achieved with a solid loading (SL) of 0.2% (0.1 g / 50 ml), 0.4% (0.2g/50ml), and 0.6% (0.3g/50ml). Dispersion was achieved using ultrasound. After the dispersion is prepared, repeated dip coating up to 5 times was tested. A minimum of two dip coats are needed to achieve the minimum roughness for superhydrophobic behavior (after all steps are completed). More than 5 cycles can also be done, however, the higher the number of cycles the less transparent the samples will be.

Silica sol-gel deposition

Base on the result shown in the last paragraph, a minimum of two dip coats are needed to achieve the minimum roughness for superhydrophobic behavior (after perfluoro silane coating completed). Glass slides with nanoparticles on surface were dipped in silica-sol - ethanol solution with different ratio (1%~5%). Then withdrawn at a speed of 1.5cm/1s by dip coater and were dried in air for 24hrs.

Self-assembled monolayer deposition-hydrophobization

Chemical used for third deposition layer was heptadecafluorodecyltrichlorosilane purchased from Gelest Inc. However, there are other chemicals which could contribute the similar property. For example, fluorinated alkyl-silane and alkyl silane (greater than C8 is preferable). The third layer has been done successfully with the concentration 0.2% ~0.5% of fluorinated silane in chloroform.

Results and Discussion

Initial Contact Angle Measurement

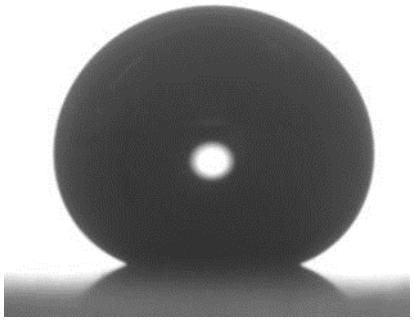

Figure 4-2. Contact angle image for sample with 69V% of particle. (Photo courtesy of author)

Varying concentration of silica sol results in different thickness of cover layer. In our prediction, this cover layer should be thin enough to prevent burring silica nanoparticle layer. However, if this layer is too thin, the mechanical strength enhancement would be insignificant. Threshold value was found at 60V% to 70V% with drawing speed 1.5cm/1s of dipped coater.

Figure 4-2 is the 69V% sample's contact angle measure by Rame-Hart goniometer. Initial contact angle of 69V% samples is 153±2°.

Contact Angle Change against Abrasion Cycles

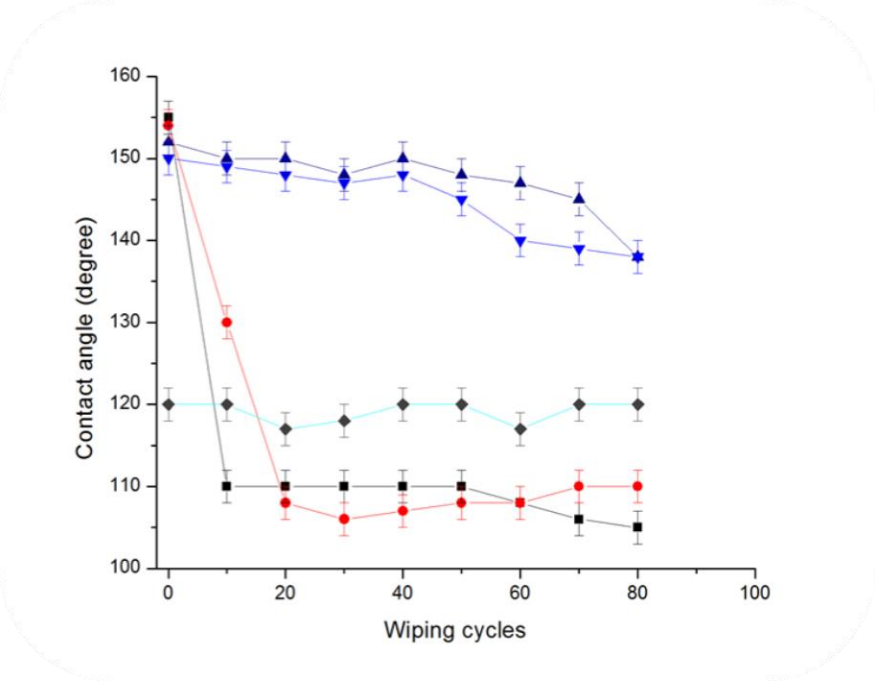

Figure 4-3. Contact angle change with wiping cycles increase for samples with different silica particles volume percent (■: 87V%, ●: 77V%, ▲:69V%, ▼: 62.5V%, ♦:57V%)

In order to understand the wear resistance of these transparent superhydrophobic samples, durability test was run by linear abraser model 5700 manufactured by TABER industry and the abrasive is windshield wiper manufactured by BOSCH and loading is 20g. This loading is close to the value that wind shield wiper applied on windshield. Figure 4-3 lists change of contact angle (CA) with different wiping cycles for samples with particle volume percent, which is from (57V% to 87V%). As we can see, after 10 cycles wiping, CA of weak coating samples drop, e.g. 87V% and 77V%, to around 115° which is the intrinsic contact angle of heptadecafluorodecyl-trichlorosilane. It means that the surface roughness has been destroyed. By contrast, durable coating, e.g. 62V% and 69V%, could resist at least 70 wiping cycles and contact angle is still

above 150°. This is the threshold value we are seeking and fulfill our prediction, which is 60V% to 70V%.

Transmittance Measurement

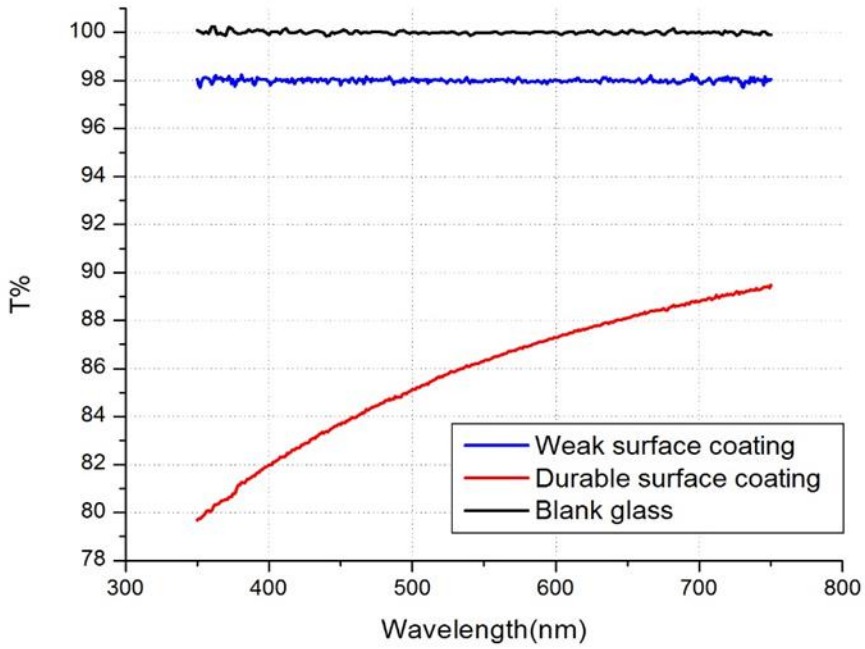

Figure 4-4. Transmittance vs. wavelength with black glass, weak surface coating, and durable surface coating

Transmittance was measured by the UV/Visible Perkin Elmer Lambda800. Figure 4-4 shows the transmittance (T %) of the durable (69V%) and weak (87%) coating samples compared to the blank reference glass slide. From the Figure 4-4, weak coatings have 98% transmittance in the visible light wavelength (400-700nm). However, durable coatings only possess 82%~90% transmittance. Although there is a 10% discrepancy between these two samples, Figure 4-5 shows the transparency observed by the bare eye. The word on the sheet still distinguishable through two kinds of coating.

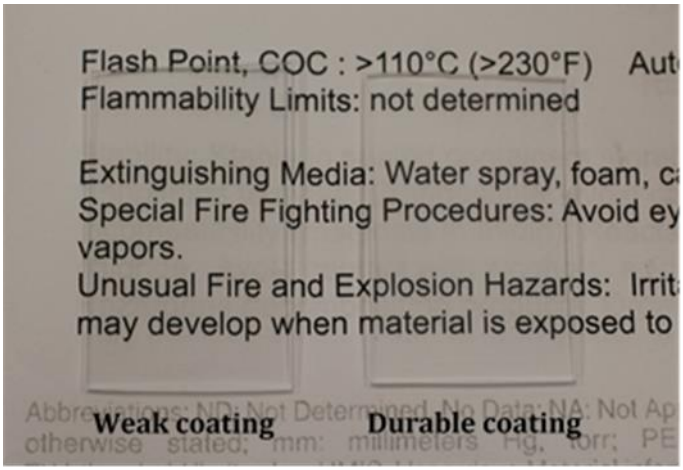

Figure 4-5. Camera photo for weak (87V%) and durable (69%) coating. (Photo courtesy of author)

Summary

Transparent superhydrophobic coating was attained by silica nanoparticles stacking and then further undergoing hydrophobization process. Other reports also achieved transparent superhydrophobic coating with similar approaches. However, it's much more arduous to enhance transparent superhydrophobic coating because particle layers should be stacked regularly and thickness should be small. Any particle agglomeration or cluster strongly impacts the transmittance of coating because of light scattering. In Chapter 4, we provide an idea about securing nanoparticle stacking by covering a layer of silica gel. This silica sol-gel layer should be present along the surface of nanoparticle. If too thin, fortification of structure is not obvious. Conversely, if too thick, roughness factor will decrease dramatically and superhydrophobicity will vanish. Concentration of silica-sol was adjusted to control the thickness of silica cover layer. A durable superhydrophobic coating was attained and this coating remained superhydrophobic until 80 times of abrasion which is 500%~600% enhancement comparing to weak coating.

CHAPTER 5
FABRICATION OF DURABLE SUPERHYDROPHOBIC AND TRANSPARENT COATING VIA SILANE COUPLING AGENTS

Introduction

In Chapter 4, sol-gel layer was introduced to cover the deposited silica nanoparticles and intended to improve strength of surface feature. However, sol-gel cover layer is only a physical enhancement which means that there is no chemical reaction occurring between cover layer and deposited particles. In Chapter 4, silane coupling agent is brought to be a linker between nanoparticles and whole coating material could be regarded as a particles- oligomer composite. This design is similar to the concept of durable superhydrophobic paint. However, transparency issue results in a complicated fabrication process because particle agglomeration strongly influences the light scattering yield. So transparent superhydrophobic coatings are not being able to build up in one step like non-transparent system. In Chapter 5, 3-mercappropyl trimethoxysilane (MPTMS) was used as the silane coupling agent in order to connect each particle. Silica nanoparticles were chosen to be surface roughness contributor. After reacted with MPTMS, silica nanoparticles would turn to thiol group terminated and named as M-particles. Glass slide was also treated with MPTMS and named as M-Glass. Multilayer M-particles were deposited on M-glass and whole system was oxidized by hydrogen peroxide and thiol-disulfide reaction was triggered by appropriate catalyzed environment. Thiol-disulfide reaction occurred between M-particles and particle-glass slide. An oligomer-particles composite was achieved in this method. Ultimately, heptadecafluoro-1, 1, 2, 2,-tetrahydrodecyltrichlorosilcane was used to hydrophobized surface. Strength- enhanced translucent superhydrophobic coating was attained.

Background

Silane Coupling Agents

Silane coupling agents have been used to bond organic and inorganic material. Figure 5-1 is the general formula of silane coupling agents and there two terminations in silane coupling agent formula which are organic functional group (R-side) and hydrolyzable group (X side). Typical X side functional groups are alkoxy, acyloxy, halogen or amine and this side aims to the hydroxyl group (-OH) on the surface of metal oxide. These leaving groups possess different dissociation energies and byproducts. In Figure 5-2, Gelest Inc. listed dissociation energies for common leaving groups and researchers could select desired X side depending on experimental requirement. In general, reactivity decreases in the order: Si-NR2 > Si-Cl > Si-NH-Si > Si-O2CCH3 > Si-OCH3 > Si-OCH2CH3[70] .On the other hand, selections of R-side are bountiful such as acrylate, epoxy amine, or mercapto etc. With R-side existing, plenty of chemical reaction could be triggered by specific oxidation or catalyzed environment.

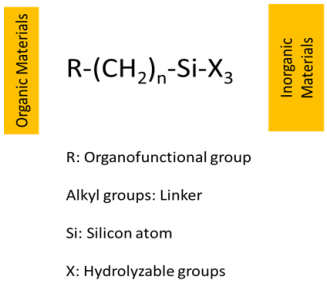

Figure 5-1. Common formula of silane coupling agents

Bond	Dissociation Energy Kcal/mole
Me3Si-NMe2 (dimethyamine)	98
Me3Si-N(SiMe3)2 tris(dimethylamino)	109
Me3Si-Cl (chloro)	117
Me3Si-OMe (methoxy)	123
Me3Si-OEt (ethoxy)	122

Figure 5-2. Dissociation energy of X-Side leaving group, from Gelest Inc. [41].

Strategy to Bond Nanoparticles and Glass Surface

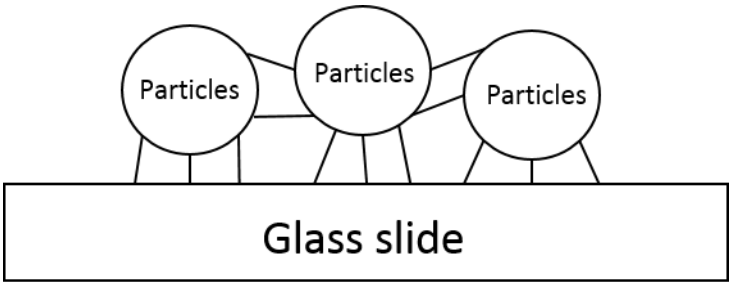

Figure 5-3. Schematic of a silicon oxide particle bonded to glass surface via oligomer chain.

Because of the versatility of R side of silane coupling agents, we could choose any two kind of silane which can react to each other. For example, amine-epoxide, thiol-epoxide, or thiol-thiol. Here, mercaptopropyl trimethoxysilane (MPTMS) was selected to synthesize thiol-terminated particles or glass slide surface. Figure 5-2 illustrates the oligomer chain formation of glass-particle, particle-particle interface. Particles and glass slide were pre-treated with MPTMS, and then thiol terminated particles were deposited on the thiol-terminated glass slide. Subsequently, immerse whole system into hydrogen peroxide oxidation bath and thiol-disulfide reaction would be activated and disulfide bond would be formed between particles and particle-glass interface.

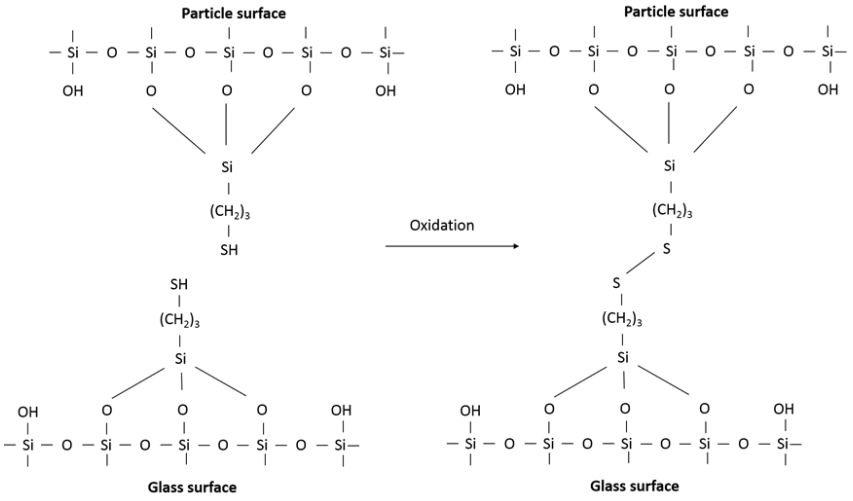

Figure 5-4. Schematic of thiol-disulfide bond formation between silica particle and glass slide

Thiol-disulfide reaction

Masayuki et al [71] claimed an oxidation environment and catalyst for benzyl mercaptan to dibenzyl disulfide. In the report, thiol-disulfide reaction was activated by hydrogen peroxide-ethyl acetate solution. They also reported 3 catalysts and corresponding yields and reaction times. Relying on their results, NaI was chosen as a catalyst in our thiol-disulfide reaction.

Conjugation of thiol group after oxidation

In Figure 5-4 [72], thiol (R-SH) can be oxidized by two electrons to sulfenic acid (RSOH). Furthermore, R-SOH can form disulfide bond with other thiol or react with another sulfenic acid and yield thiosulfinate (RS (O) SR'). These two reactions occurred on the border of two thiol-terminated particles or of thiol-terminated particle and glass. Durability of coating was enhanced by these inner chemical bonds like Figure 5-2. On the other hand, from the Figure 5-4, with excess oxidant, sulfenic acid could be further oxidized to sulfinic acid (RSO2H) or even sulfonic acid (RSO3H). There is hydroxyl group existing in these three groups, so further hydrophobization process still can be conducted.

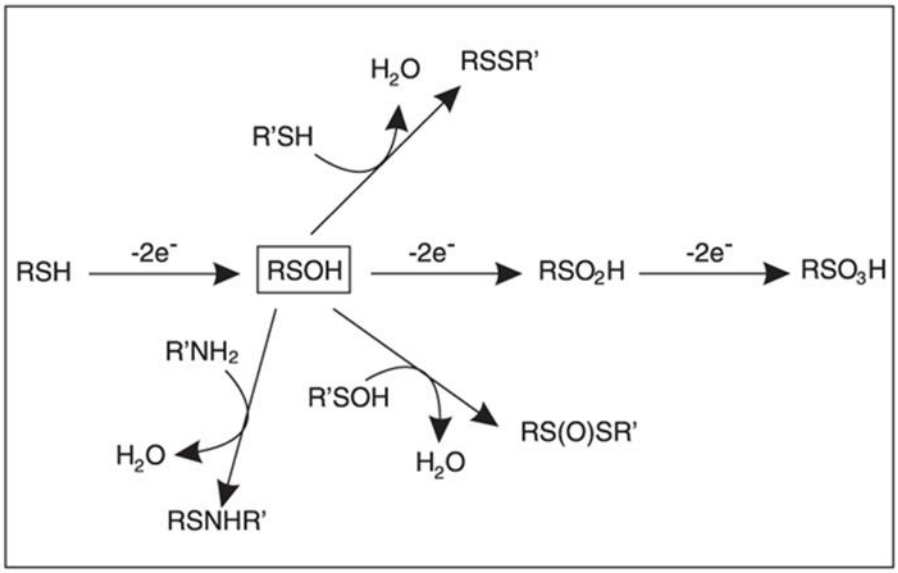

Figure 5-5. Formation and reactions of sulfenic acid [72]

Materials and Methods

Silica nanoparticles synthesis (Stöber process)

Stöber process was used to synthesize silica nanoparticles with 40nm diameter. 8.33g of tetra ethyl silicate (TEOS), 5g of de-ionized water, and 0.98g of 0.28N aqueous ammonium hydroxide solution were added to 100ml 99% ethanol and agitated for 24hours at 50°C. This process generated monodisperse silica nanoparticles of ~40 nm, as measure by SEM.

Preparation of thiol-terminated silica nanoparticles

40nm silica nanoparticles were dispersed in acetone by ultra-sonication for 1 hr. and the ratio of silica particles in acetone was 0.2g in 50ml acetone. 100µl MPTMS was added into silica dispersion and waited for 1hr. Thiol-terminated silica particles were obtained in this way and named as T-particles. MPTMS was purchased from Sigma-Aldrich with 99% concentration.

Preparation of thiol-terminated glass slide

Glass slide was immersed in isopropanol and ultrasonicated for 30mins and the goal of this procedure is to clean contamination. Furthermore, glass slide was immersed in piranha solution for 30 mins and then flushed by DI water. The goal of piranha solution is to oxidize glass surface and enlarge the density of hydroxyl group on the silica particles. By doing this, more MPTMS could be bonded on the SiO2 particles and this results in more silane bonding chains forming in whole coating material. After treating with piranha solution, glass slide was immersed in 30ml acetone and 100µl MPTMS was added and waited for 30mins. Dried at 120° in an oven for 15mins and contact angle of glass slide was measured here to verify MPTMS bonding. Glass slide was named T-glass after water contact angle was over 50° which is the empirical value that other reports said.

Deposit T-particles on T-glass

0.2g T-particles were dispersed in acetone and ultrasonicated for 1 hr. Afterward, T-glass slide was dipped into T-particle dispersion and withdrawn with speed 85mm/min.This process was repeated for 3 times in order to establish sufficient roughness. Then sample was dried in air for 1hr.

Thiol-disulfide oxidation

Sample was dipped into ethyl acetate solution with varied amount of NaI 1mol% aqueous solution and hydrogen peroxide. The reaction time was 30 mins. Concentration of NaI aqueous solution and H_2O_2 is strongly affect whether the thiol-disulfide bond can be activated or not and corresponding results were listed in the following paragraphs

Hydrophobization

Samples were dipped into heptadecafluorodecyltrichlorosilane-chloroform solution with ratio 0.2% ~0.5%. Chemical used for hydrophobization was purchased from Gelest Inc. Reaction time is 30 mins and in room temperature. Then, sample was dried in 120°C oven for 1hr.

Results and Discussion

Wear Resistance of Samples with Different Oxidation Condition

After T particles were deposited on T glass, thiol to disulfide reaction was conducted. However, because oxidation environment was unknown yet, reaction time and concentration are the parameters and a series of experiments have been done and reported in the Figure 5-6 and Figure 5-7. In Figure 5-6, reaction time was set as 24 hrs. and concentrations of H_2O_2 and NaI are varied and shown in this formula:

$$X\ 1mol\%\ NaI(aq) + Y\ 30\%\ H_2O_2 + 30ml\ EtAc$$

Amount of EtAC was fixed to 30ml and X means the adding amount of 1mol% NaI aqueous solution. Y presents the adding amount of 30% hydrogen peroxide. After 24hrs reaction,

samples were treated by fluorinated silane in chloroform solution and dried in 120° oven. Water contact angle was measured.

In Figure 5-6, ratio of X: Y was anchored in 1:1 but their concentration was adjusted. From the results, 4 samples show unstable contact angle. Basically, coatings were wiped out in 10 abrasion cycles although they possess superhydrophobicity at beginning. We hypothesized the reaction time was too long so the reaction time was reduced to 30mins. The outcome is shown in Figure 5-7. Once the reaction time was reduced to 30mins, coating was sturdier than samples with 24hrs reaction time. Figure 5-8 shows how contact angle decreases against wind shield wiper abrasion. Samples with 30mins oxidation stay superhydrophobic until 40 cycles and contact angle drops to 110° after 70 cycles which means surface structure was not ruined totally until 70 cycles. Strength of surface structure was elevated by silane coupling agent.

X: NaI , Y: H_2O_2	Initial contact angle and durability
X: 1ml , Y: 1ml	CA is 153° ± 3° but drop to 105°± 3° after 10 cycles wind-shield wiper rubbing
X: 500 µL , Y: 500 µL	CA is 152° ± 3° but drop to 105°± 3° after 10 cycles wind-shield wiper rubbing
X: 200 µL , Y: 200 µL	CA is 154° ± 3° but drop to 105°± 3° after 10 cycles wind-shield wiper rubbing
X: 50 µL , Y: 50 µL	CA is 155° ± 3° but drop to 105°± 3° after 10 cycles wind-shield wiper rubbing

Figure 5-6. Diverse X,Y amount don't influence durability of coating – reaction time 24hrs

X: NaI , Y: H_2O_2	Initial contact angle and durability
X: 50 µL, Y: 50 µL	CA is 158° ± 3° but drop to 105°± 3° after **70** cycles wind-shield wiper rubbing

Figure 5-7. Reduced oxidation time enhanced the durability of coating-reaction time 30 mins

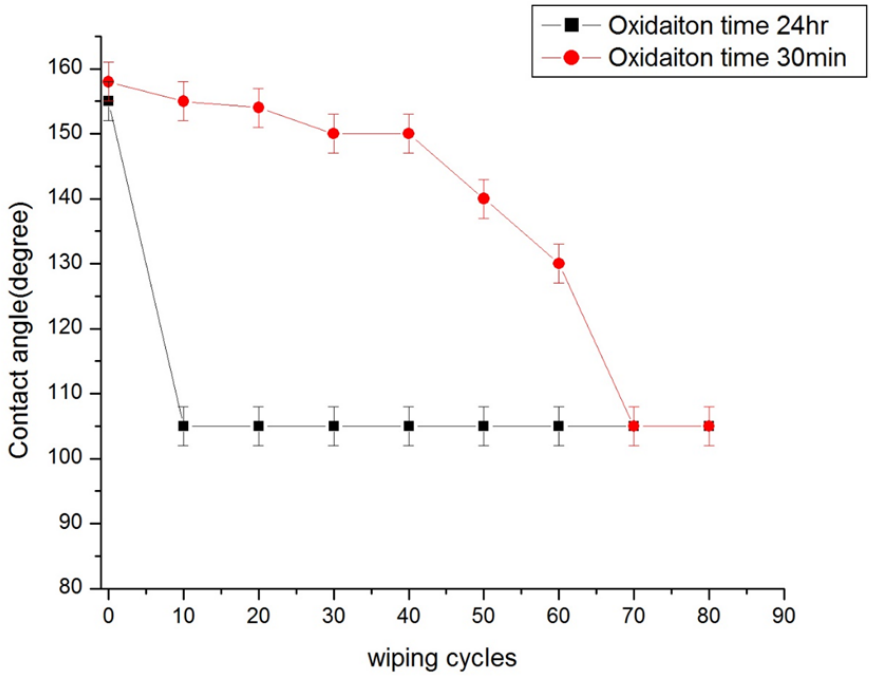

Figure 5-8. Contact angle change against abrasion cycles (■: X: 50µl, Y: 50 µl, reaction time: 24hrs; ●: X: 50µl, Y: 50 µl, reaction time: 30mins)

Summary

Silica nanoparticles were treated by MPTMS and turned to thiol termination. With this functionality, thiol-disulfide reaction could be triggered in specific oxidation condition. Strength of coating could be enhanced by disulfide bond on particle-particle interface and particle-glass interface. This idea the similar to our durable superhydrophobic coating. Whole coating is fortified by inner polymer web like structure. After hydrophobization, fluffy structure became superhydrophobic and with fair strength which can possess superhydrophobicity after 70 times abrasion by wind-shield wiper. This is the first quantitative data to describe the wear resistance of transparent superhydrophobic coating. With this idea, other sorts of silane coupling agents also could be used to construct inter-particle connection.

CHAPTER 6
CONCLUSION

Superhydrophobic material seized researchers' attention due to its versatile properties such as self-cleaning, anti-fouling, and ice phobicity. However, after many years of development, researchers discovered SH material could only be fabricated in small scale and the structure was very vulnerable. The reason is that surface roughness is an essential factor to achieve superhydrophobicity. Although some reports claimed durable superhydrophobic material has been made, there was not a standard test to quantify the durability withstand wear. Therefore, this dissertation provides a recommendation for the standardization of how wear resistance measurements should be taken for superhydrophobic materials, in reference to ASTM standards (ASTM D4060 – 14).

Moreover, in order to prevail over durability issue of superhydrophobic material, this dissertation proposed a novel design which differs from traditional ways. A volumetric superhydrophobic coating was introduced to overcome the adversity of superhydrophobic material. Fluorinated particles were secured by polymer binder in funicular structure and whole coating became fluffy and provided high roughness.

Our system is based on a polymethyl methacrylate-polyvinylidene difluoride (PMMA-PVDF) polymer blend, acting as a thermoplastic binder, and hydrophobized metal oxide particles, which develop surface roughness. By varying the V% of pigments, thresholds to achieve superhydrophobicity was demonstrated in the range of 60V% to 70V% particle volume percent. This range is the transition point between capillary structure to funicular structure and the maximum packing density of random close packing. A dramatic change of CDR was also observed in this range to prove the explanation of structure transition. Higher V% of pigments results in a weaker structure but possesses higher initial contact angle. So there is a trade-off here

and that's why threshold to just achieve superhydrophobicity is essential. With the data, researchers know which V% of pigment should be added and this will turn out a superhydrophobic coating with sturdiest structure

In terms of durability of coating, samples with 60%~70% V% of pigments expressed lowest CDR and could resist 1000 abrasion cycles by metallurgy sand paper and order to strengthen the applicability, formulating this coating as a paint allows for application into large areas, and the ability to select color, which are white, black, blue, green and red.

On the other hand, another shortcoming of SH material is the transmittance. This dissertation followed the consequences in the durable paint fabrication system and substitute pigment to monodisperse silica particle and binder to inorganic silica gel. Threshold to achieve superhydrophobicity was also found in the range of 60V% to 70V%. Sample 62V% and 69V% retained in superhydrophobic regime in after 80 times abrasions by windshield wiper.

This dissertation provides two measurements to quantify the durability of superhydrophobic material and a novel design to fabricate the durable superhydrophobic material as well. We hope this versatile material could be used widely in the future.

LIST OF REFERENCES

[1] U. Mock, R. Förster, W. Menz, and J. Rühe, "Towards ultrahydrophobic surfaces: a biomimetic approach," *J. Phys. Condens. Matter*, vol. 17, no. 9, pp. S639–S648, Mar. 2005.

[2] T. Onda, S. Shibuichi, N. Satoh, and K. Tsujii, "Super-Water-Repellent Fractal Surfaces," *Langmuir*, vol. 12, no. 9, pp. 2125–2127, Jan. 1996.

[3] A. Otten and S. Herminghaus, "How Plants Keep Dry: A Physicist's Point of View," *Langmuir*, vol. 20, no. 6, pp. 2405–2408, Mar. 2004.

[4] S. Pan, A. K. Kota, J. M. Mabry, and A. Tuteja, "Superomniphobic Surfaces for Effective Chemical Shielding.," *J. Am. Chem. Soc.*, vol. 135, no. 2, pp. 578–81, Jan. 2013.

[5] A. Tuteja, W. Choi, M. Ma, J. M. Mabry, S. A. Mazzella, G. C. Rutledge, G. H. McKinley, and R. E. Cohen, "Designing Superoleophobic Surfaces," *Science (80-.).*, vol. 318, pp. 1618–1622, Dec. 2007.

[6] R. N. Wenzel, "Resistance of Solid Surfaces to Wetting by Water," *Ind. Eng. Chem.*, vol. 28, no. 8, pp. 988–994, 1936.

[7] S. R. Coulson, I. Woodward, J. P. S. Badyal, S. A. Brewer, C. Willis, P. Down, and S. S. P. Ojq, "Super-Repellent Composite Fluoropolymer Surfaces," *J. Phys. Chem. B*, vol. 104, pp. 8836–8840, 2000.

[8] R. Dufour, M. Harnois, V. Thomy, R. Boukherroub, and V. Senez, "Contact angle hysteresis origins: Investigation on super-omniphobic surfaces," *Soft Matter*, vol. 7, no. 19, p. 9380, 2011.

[9] D. Ebert and B. Bhushan, "Transparent, Superhydrophobic, and Wear-Resistant Coatings on Glass and Polymer Substrates Using SiO2, ZnO, and ITO Nanoparticles.," *Langmuir*, vol. 28, no. 31, pp. 11391–9, Aug. 2012.

[10] R. Fürstner, W. Barthlott, C. Neinhuis, and P. Walzel, "Wetting and Self-Cleaning Properties of Artificial Superhydrophobic Surfaces," *Langmuir*, vol. 21, pp. 956–961, 2005.

[11] J. Genzer and K. Efimenko, "Recent developments in superhydrophobic surfaces and their relevance to marine fouling: a review," *Biofouling*, vol. 22, no. 5–6, pp. 339–60, Jan. 2006.

[12] R. J. Klein, P. M. Biesheuvel, B. C. Yu, C. D. Meinhart, and F. F. Lange, "Producing Super-Hydrophobic Surfaces with Nano-Silica Spheres," *Zeitschrift für Met.*, vol. 94, no. 48, pp. 377–380, 2003.

[13] K. Koch, B. Bhushan, Y. C. Jung, and W. Barthlott, “Fabrication of artificial Lotus leaves and significance of hierarchical structure for superhydrophobicity and low adhesion,” *Soft Matter*, vol. 5, no. 7, p. 1386, 2009.

[14] H. Zhang, R. Lamb, and J. Lewis, “Engineering nanoscale roughness on hydrophobic surface - Preliminary assessment of fouling behaviour,” in *Science and Technology of Advanced Materials*, 2005, vol. 6, no. 3–4 SPEC. ISS., pp. 236–239.

[15] R. J. Daniello, N. E. Waterhouse, and J. P. Rothstein, “Drag reduction in turbulent flows over superhydrophobic surfaces,” *Phys. Fluids*, vol. 21, no. 8, 2009.

[16] S. Wang and L. Jiang, “Definition of Superhydrophobic States,” *Adv. Mater.*, vol. 19, pp. 3423–3424, 2007.

[17] A. Tuteja, W. Choi, J. M. Mabry, G. H. McKinley, and R. E. Cohen, “Robust omniphobic surfaces,” *Proc. Natl. Acad. Sci. USA*, vol. 105, no. 47, pp. 18200–5, Nov. 2008.

[18] J. Bico, C. Marzolin, and D. Quéré, “Pearl drops,” *Europhys. Lett.*, vol. 47, no. 2, pp. 220–226, 2007.

[19] D. Quéré, “Non-sticking drops,” *Reports Prog. Phys.*, vol. 68, no. 11, pp. 2495–2532, 2005.

[20] J. Bico, U. Thiele, and D. Quéré, “Wetting of textured surfaces,” in *Colloids and Surfaces A: Physicochemical and Engineering Aspects*, 2002, vol. 206, no. 1–3, pp. 41–46.

[21] D. Murakami, H. Jinnai, and A. Takahara, “Wetting transition from the cassie-baxter state to the wenzel state on textured polymer surfaces,” *Langmuir*, vol. 30, no. 8, pp. 2061–2067, 2014.

[22] S. H. Hsu, K. Woan, and W. Sigmund, “Biologically inspired hairy structures for superhydrophobicity,” *Mater. Sci. Eng. R Reports*, vol. 72, no. 10, pp. 189–201, 2011.

[23] P. Roach, N. J. Shirtcliffe, and M. I. Newton, “Progess in superhydrophobic surface development,” *Soft Matter*, vol. 4, no. 2, p. 224, 2008.

[24] J. T. Simpson, S. R. Hunter, and T. Aytug, “Superhydrophobic materials and coatings: a review,” *Reports Prog. Phys.*, vol. 78, no. 8, p. 086501, 2015.

[25] J. Bravo, L. Zhai, Z. Wu, R. E. Cohen, and M. F. Rubner, “Transparent superhydrophobic films based on silica nanoparticles,” *Langmuir*, vol. 23, no. 13, pp. 7293–7298, 2007.

[26] X. Y. Ling, I. Y. Phang, G. J. Vancso, J. Huskens, and D. N. Reinhoudt, “Stable and transparent superhydrophobic nanoparticle films,” *Langmuir*, vol. 25, no. 5, pp. 3260–3263, 2009.

[27] A. Nakajima, A. Fujishima, K. Hashimoto, and T. Watanabe, “Preparation of transparent superhydrophobic boehmite and silica films by sublimation of aluminum acetylacetonate,” *Adv. Mater.*, vol. 11, no. 16, pp. 1365–1368, 1999.

[28] A. Nakajima, K. Hashimoto, T. Watanabe, K. Takai, G. Yamauchi, and A. Fujishima, “Transparent superhydrophobic thin films with self-cleaning properties,” *Langmuir*, vol. 16, no. 17, pp. 7044–7047, 2000.

[29] H. M. Shang, Y. Wang, S. J. Limmer, T. P. Chou, K. Takahashi, and G. Z. Cao, “Optically transparent superhydrophobic silica-based films,” *Thin Solid Films*, vol. 472, no. 1–2, pp. 37–43, 2005.

[30] G. Wang, H. Wang, and Z. Guo, “A robust transparent and anti-fingerprint superhydrophobic film,” *Chem. Commun. (Camb).*, vol. 49, no. 66, pp. 7310–2, 2013.

[31] S. Höhne, C. Blank, A. Mensch, M. Thieme, R. Frenzel, H. Worch, M. Müller, and F. Simon, “Superhydrophobic alumina surfaces based on polymer-stabilized oxide layers,” *Macromol. Chem. Phys.*, vol. 210, no. 16, pp. 1263–1271, 2009.

[32] Y. Xiu, Y. Liu, D. W. Hess, and C. P. Wong, “Mechanically robust superhydrophobicity on hierarchically structured Si surfaces.,” *Nanotechnology*, vol. 21, no. 15, p. 155705, 2010.

[33] T. Yanagisawa, A. Nakajima, M. Sakai, Y. Kameshima, and K. Okada, “Preparation and abrasion resistance of transparent super-hydrophobic coating by combining crater-like silica films with acicular boehmite powder,” *Mater. Sci. Eng. B Solid-State Mater. Adv. Technol.*, vol. 161, no. 1–3, pp. 36–39, 2009.

[34] Y. Li, L. Li, and J. Sun, “Bioinspired Self-Healing Superhydrophobic Coatings,” *Angew. Chemie*, vol. 122, no. 35, pp. 6265–6269, 2010.

[35] A. Solga, Z. Cerman, B. F. Striffler, M. Spaeth, and W. Barthlott, “The dream of staying clean: Lotus and biomimetic surfaces.,” *Bioinspir. Biomim.*, vol. 2, no. 4, pp. S126–S134, 2007.

[36] J. Zimmermann, F. A. Reifler, G. Fortunato, L. C. Gerhardt, and S. Seeger, “A simple, one-step approach to durable and robust superhydrophobic textiles,” *Adv. Funct. Mater.*, vol. 18, no. 22, pp. 3662–3669, 2008.

[37] B. B. J. Basu and A. K. Paranthaman, “A simple method for the preparation of superhydrophobic PVDF-HMFS hybrid composite coatings,” *Appl. Surf. Sci.*, vol. 255, no. 8, pp. 4479–4483, 2009.

[38] B. Bhushan, Y. C. Jung, and K. Koch, “Micro-, nano- and hierarchical structures for superhydrophobicity, self-cleaning and low adhesion.,” *Philos. Trans. A. Math. Phys. Eng. Sci.*, vol. 367, no. 1894, pp. 1631–1672, 2009.

[39] X. Deng, L. Mammen, H.-J. Butt, and D. Vollmer, “Candle Soot as a Template for a Transparent Robust Superamphiphobic Coating,” *Science (80-.).*, vol. 335, no. 6064, pp. 67–70, 2012.

[40] A. Steele, I. Bayer, and E. Loth, “Inherently superoleophobic nanocomposite coatings by Spray Atomization,” *Nano Lett.*, vol. 9, no. 1, pp. 501–505, 2009.

[41] Z. Cui, Q. Wang, Y. Xiao, C. Su, and Q. Chen, “The stability of superhydrophobic surfaces tested by high speed current scouring,” *Appl. Surf. Sci.*, vol. 254, no. 10, pp. 2911–2916, 2008.

[42] T. Verho, C. Bower, P. Andrew, S. Franssila, O. Ikkala, and R. H. A. Ras, “Mechanically Durable Superhydrophobic Surfaces,” *Adv. Mater.*, vol. 23, no. 5, pp. 673–678, 2011.

[43] M. Manca, A. Cannavale, L. De Marco, A. S. Aric??, R. Cingolani, and G. Gigli, “Durable superhydrophobic and antireflective surfaces by trimethylsilanized silica nanoparticles-based sol-gel processing,” *Langmuir*, vol. 25, no. 11, pp. 6357–6362, 2009.

[44] X. Liu, Y. Xu, K. Ben, Z. Chen, Y. Wang, and Z. Guan, “Transparent, durable and thermally stable PDMS-derived superhydrophobic surfaces,” *Appl. Surf. Sci.*, vol. 339, pp. 94–101, 2015.

[45] L. Ionov and A. Synytska, “Self-healing superhydrophobic materials,” *Phys. Chem. Chem. Phys.*, vol. 14, no. 30, pp. 10497–10502, 2012.

[46] H. Wang, Y. Xue, J. Ding, L. Feng, X. Wang, and T. Lin, “Durable, self-healing superhydrophobic and superoleophobic surfaces from fluorinated-decyl polyhedral oligomeric silsesquioxane and hydrolyzed fluorinated alkyl silane,” *Angew. Chemie - Int. Ed.*, vol. 50, no. 48, pp. 11433–11436, 2011.

[47] L. Wu, J. Zhang, B. Li, and A. Wang, “Mechanical- and oil-durable superhydrophobic polyester materials for selective oil absorption and oil/water separation,” *J. Colloid Interface Sci.*, vol. 413, pp. 112–117, 2014.

[48] Z. Zhang, B. Ge, X. Men, and Y. Li, “Mechanically durable, superhydrophobic coatings prepared by dual-layer method for anti-corrosion and self-cleaning,” *Colloids Surfaces A Physicochem. Eng. Asp.*, vol. 490, pp. 182–188, 2016.

[49] C. Du, J. Wang, Z. Chen, and D. Chen, “Durable superhydrophobic and superoleophilic filter paper for oil-water separation prepared by a colloidal deposition method,” *Appl. Surf. Sci.*, vol. 313, pp. 304–310, 2014.

[50] F. Wang, S. Yu, J. Ou, M. Xue, and W. Li, “Mechanically durable superhydrophobic surfaces prepared by abrading,” *J. Appl. Phys.*, vol. 114, no. 12, 2013.

[51] W. Conshohocken, “Standard Test Method for Abrasion Resistance of Organic Coatings by the Taber,” *North*, vol. 06, pp. 6–8, 1995.

[52] F. Gabrieli, P. Lambert, S. Cola, and F. Calvetti, “Micromechanical modelling of erosion due to evaporation in a partially wet granular slope,” *Int. J. Numer. Anal. Methods Geomech.*, vol. 36, no. 7, pp. 918–943, 2012.

[53] V. Baranau and U. Tallarek, “Random-close packing limits for monodisperse and polydisperse hard spheres.,” *Soft Matter*, vol. 10, pp. 3826–41, 2014.

[54] F. A.L. Dullien, *Porous Media , Fluid transport and pore structure*. 1992.

[55] G. T. Nolan and P. E. Kavanagh, “Random packing of nonspherical particles,” *Powder Technol.*, vol. 84, no. 3, pp. 199–205, 1995.

[56] C. Radin, “Random close packing of granular matter,” *J. Stat. Phys.*, vol. 131, no. 4, pp. 567–573, 2008.

[57] G. D. Scott and D. M. Kilgour, “The density of random close packing of spheres,” *J. Phys. D. Appl. Phys.*, vol. 2, no. 6, pp. 863–866, 2002.

[58] A. T. Young, “Rayleigh scattering,” *Phys. Today*, vol. 35, no. January, pp. 42–48, 1982.

[59] A. Bucholtz, “Rayleigh-Scattering Calculations for the Terrestrial Atmosphere,” *Appl. Opt.*, vol. 34, no. 15, pp. 2765–2773, 1995.

[60] H. Du, “Mie-scattering calculation,” *Appl. Opt.*, vol. 43, no. 9, pp. 1951–1956, 2004.

[61] R. M. Drake, “Mie scattering,” *Am. J. Phys.*, vol. 53, no. 10, p. 955, 1985.

[62] I. S. Saidi, S. L. Jacques, and F. K. Tittel, “Mie and Rayleigh modeling of visible-light scattering in neonatal skin.,” *Appl. Opt.*, vol. 34, no. 31, pp. 7410–7418, 1995.

[63] W. Stöber, A. Fink, and E. Bohn, “Controlled growth of monodisperse silica spheres in the micron size range,” *J. Colloid Interface Sci.*, vol. 26, no. 1, pp. 62–69, 1968.

[64] R. K. Iler, *The chemistry of silica: solubility, polymerization, colloid and surface properties, and biochemistry*. 1979.

[65] C. J. Brinker, G. C. Frye, A. J. Hurd, and C. S. Ashley, “Fundamentals of sol-gel dip coating,” *Thin Solid Films*, vol. 201, no. 1, pp. 97–108, 1991.

[66] C. J. Brinker and G. W. Scherer, *Sol-Gel Science*. 1990.

[67] L.E.Scriven, *Better Ceramics Through Chemistry III*. .

[68] C. Jeffrey Brinker and A. J. Hurd, “Fundamentals of sol-gel dip-coating,” *J. Phys. III*, vol. 4, no. 7, pp. 1231–1242, 1994.

[69] I. Strawbridge and P. F. James, “Thin silica films prepared by dip coating,” *J. Non. Cryst. Solids*, vol. 82, no. 1–3, pp. 366–372, 1986.

[70] 2nd edition Gelest product handbook, A survey of properties and chemistry, *Hydrophobicity, Hydrophilicity and Silane Surface Modification*. .

[71] M. Kirihara, Y. Asai, S. Ogawa, T. Noguchi, A. Hatano, and Y. Hirai, "A mild and environmentally benign oxidation of thiols to disulfides," *Synthesis (Stuttg).*, no. 21, pp. 3286–3289, 2007.

[72] L. Turell, S. Carballal, H. Botti, R. Radi, and B. Alvarez, "Oxidation of the albumin thiol to sulfenic acid and its implications in the intravascular compartment," *Brazilian Journal of Medical and Biological Research*, vol. 42, no. 4. pp. 305–311, 2009.

BIOGRAPHICAL SKETCH

Yung-Chieh was born in Kaohsiung City, Taiwan. He obtained his Bachelor of Material Science and Engineering from National Cheng Kung University (NCKU) in Tainan City, Taiwan. He attended the University of Florida starting in August 2012 in a master's program and transferred to the doctorate program on May 2013 by Dr. Wolfgang Sigmund. During the time of pursuing his PhD, he has applied 8 patents about development of durable superhydrophobic coating.